

Theme Va: Structural behaviour including hybrid construction

Objekttyp: **Group**

Zeitschrift: **IABSE congress report = Rapport du congrès AIPC = IVBH
Kongressbericht**

Band (Jahr): **10 (1976)**

PDF erstellt am: **08.08.2024**

Nutzungsbedingungen

Die ETH-Bibliothek ist Anbieterin der digitalisierten Zeitschriften. Sie besitzt keine Urheberrechte an den Inhalten der Zeitschriften. Die Rechte liegen in der Regel bei den Herausgebern.

Die auf der Plattform e-periodica veröffentlichten Dokumente stehen für nicht-kommerzielle Zwecke in Lehre und Forschung sowie für die private Nutzung frei zur Verfügung. Einzelne Dateien oder Ausdrucke aus diesem Angebot können zusammen mit diesen Nutzungsbedingungen und den korrekten Herkunftsbezeichnungen weitergegeben werden.

Das Veröffentlichen von Bildern in Print- und Online-Publikationen ist nur mit vorheriger Genehmigung der Rechteinhaber erlaubt. Die systematische Speicherung von Teilen des elektronischen Angebots auf anderen Servern bedarf ebenfalls des schriftlichen Einverständnisses der Rechteinhaber.

Haftungsausschluss

Alle Angaben erfolgen ohne Gewähr für Vollständigkeit oder Richtigkeit. Es wird keine Haftung übernommen für Schäden durch die Verwendung von Informationen aus diesem Online-Angebot oder durch das Fehlen von Informationen. Dies gilt auch für Inhalte Dritter, die über dieses Angebot zugänglich sind.

V

Emploi des aciers à haute résistance et à protection naturelle pour les structures hautes ou à grande portée

Anwendung hochfester Stähle, inklusive wetterfester Stähle, für hohe und weitgespannte Tragwerke

Application of high-strength Steels including weathering Steels to high-rise and long-span Structures

Va

Comportement sous charges en incluant les constructions hybrides

Tragverhalten, einschliesslich hybride Tragwerke

Structural Behaviour including Hybrid Construction

Leere Seite
Blank page
Page vide

Strength and Ductility of A572 (Grade 65) Steel Structures

La résistance et la ductilité des structures en acier A572 (grade 65)

Festigkeit und plastische Verformungsfähigkeit der Stahlkonstruktionen aus Stahl A572 (Grad 65)

S. IYENGAR

Structural Engineer
Gilbert Associates, Inc.
Reading, Pennsylvania, USA

LYNN S. BEEDLE

Director, Fritz Eng. Lab.

LE-WU LU

Professor of Civil Engineering
Lehigh University
Bethlehem, Pennsylvania, USA

1. Introduction

A572 (Grade 65) steel, a low-alloy columbium-vanadium steel, is the highest strength steel for which the use of plastic design method is permitted by the American Institute of Steel Construction Specification. The properties of this steel are specified in ASTM Specification A572-74b which covers all six grades of the A572 steel with minimum yield values of 42, 50, 55, 60, and 65 ksi.

Many of the problems encountered in the design of building frames using high strength steels relate to buckling or to instability phenomena; namely, local buckling of cross sections, instability of beam-columns, lateral-torsional buckling of beams and beam-columns, and overall instability of frames. These problems occur in structures made of low carbon steel also but become more dominant as the yield stress of the material increases.

Consider local buckling as an example. Local buckling can occur either in the flange or in the web of a cross section, depending on the width-to-thickness ratios of the elements. For steels up to 50 ksi yield, limiting ratios have been developed in order to ensure that large strains can take place without buckling. This, in turn, assures adequate deformation capacity which is one of the requirements for plastic design. The formula defining the limiting ratios, derived primarily for lower strength steels, have been extended to include high strength steels. Experimental data are needed to confirm this extension.

A research program has been carried out at Lehigh University to study the mechanical properties of the steel and the behavior of some simple structures in the inelastic range with emphasis on local and lateral buckling.

2. Tensile Properties

The required minimum tensile properties (mill tests) of A572 (Grade 65) steel are: yield point $\sigma_y = 65$ ksi, tensile strength $\sigma_u = 80$ ksi, and elongation = 15% over an 8" gage. As part of the research program, 52 tension tests were conducted, the details of which have been documented elsewhere (1).

Figure 1 shows the stress-strain curve obtained from plotting average

values of the significant quantities. The static yield stress σ_{ys} is the most important property of steel and plays a significant role in plastic design. It is the yield stress value at zero strain rate. In the tests, the machine was stopped for five minutes at a strain of approximately 0.005 in/in and σ_{ys} was recorded. Its average value was 62.1 ksi. The corresponding dynamic yield stress σ_{yd} at the testing speed of 0.025 ipm was found to be 64.6 ksi. Simulated mill tests at 0.5 ipm gave an average value of 69.3 ksi. The tensile strength σ_u averaged 85.7 ksi. The value of strain ϵ_{st} at which strain-hardening commenced was 0.0186 in/in which is about 9 times the yield strain ϵ_y . The average value of percentage elongation in 8" gage length and percentage reduction of cross-sectional area were 21.5 and 51.0 respectively.

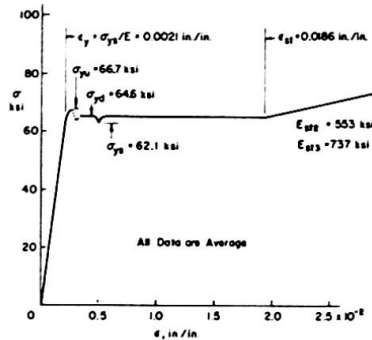


FIG. 1 IDEALIZED STRESS-STRAIN CURVE FROM TENSION TEST

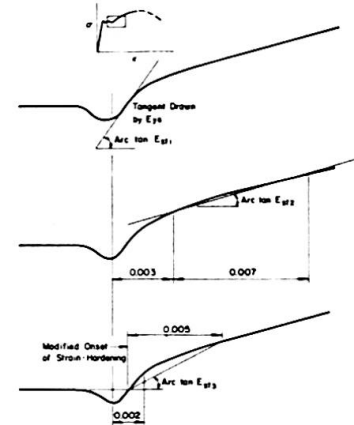


FIG. 2 SKETCH DEFINING E_{st1} , E_{st2} and E_{st3}

3. Strain-Hardening Modulus

The value of strain-hardening modulus E_{st} is important in the study of inelastic buckling of structural members. Three approaches have been used to evaluate E_{st} in this series of tests, as shown in Fig. 2. The modulus E_{st1} is the instantaneous value as measured by a tangent to the curve at the point where strain-hardening commences. This tangent is often difficult to determine consistently. Values of E_{st1} from different tests for the same material are likely to exhibit a wide scatter.

The modulus E_{st2} was measured as the chord slope between strains $\epsilon_{st}=0.003$ and $\epsilon_{st} = 0.010$. This specific range was chosen as it confines measurements to a fairly linear and stable range of the stress-strain curve and eliminates the initial erratic portion. Since measurements are made at a greater value of strain than in other methods, E_{st2} provides a conservative value.

In the "Column Research Council approach" (2), the modulus E_{st3} is the average value in the range ϵ_{st} to $\epsilon_{st} + 0.005$, where ϵ_{st} is defined as the strain corresponding to the intersection on the stress-strain curve of the yield stress level in the plastic range with the tangent to the curve in the strain-hardening range. This tangent is drawn as the average value in an increment of 0.002 in/in after the apparent onset of strain-hardening. The attempt is to eliminate the effect of the frequently encountered drop in load immediately prior to the apparent onset of strain-hardening. E_{st3} , however, includes the effect of the steep initial slope and is hence less conservative than E_{st2} .

E_{st1} values varied, in this series, from 393 ksi to 9825 ksi. The strain-hardening process in the region of strain-hardening and the inherent difficulties in determining this function have contributed to the wide scatter of values. E_{st2} values averaged 553 ksi (min. 322 ksi, max. 775 ksi). E_{st3} values ranged from 382 ksi to 1160 ksi with an average of 771 ksi.

4. Compressive Properties

Compression tests were performed on ten specimens whose dimensions were generally in accordance with ASTM standards. Minor deviations, however, were necessary in order to be able to test the full thickness of the flange or web element and still use a special strain-recording instrument of fixed gage length 0.5" in the plastic range (3).

A typical stress-strain curve is shown in Fig. 3. The average values for the three most significant quantities are: $\sigma_y = 65.14$ ksi, $\epsilon_{st} = 0.0086$ in/in, $E_{st2} = 820$ ksi. For comparison, three additional tests were performed on A441 steel specimens. The corresponding average values are: $\sigma_y = 55.8$ ksi, $\epsilon_{st} = 0.0147$ in/in, $E_{st2} = 815$ ksi.

In general, strain ϵ_{st} is smaller than in tension tests while modulus E_{st2} is larger. The higher modulus is partly due to Poisson's ratio effect since the cross-sectional area in a compression test increases. However, the increase in E_{st} is not fully accounted for even with the assumption of 0.5 for Poisson's ratio in the inelastic range.

5. Residual Stresses

Residual stresses, determined by the method of sectioning (3), in a W12 x 19 shape are shown in Fig. 4. The stresses are seen to be relatively small and there is no evidence of cold-straightening. In A36 steel, it has been found that the maximum residual stress at flange tips is about $0.3 \sigma_y$ or approximately 10 ksi (4). The present study shows that the magnitude of the maximum residual stress does not increase with yield stress level. This was also found to be true for other types of high strength steels.

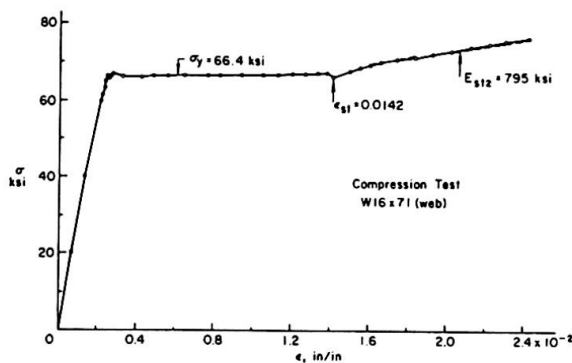


FIG. 3 STRESS-STRAIN CURVE
FROM COMPRESSION TEST

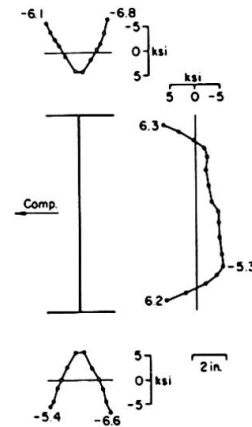


FIG. 4 RESIDUAL STRESS DISTRIBUTION IN W12 x 19 SHAPE

6. Stub Column Tests

Stub column tests were used to examine the local buckling characteristics of the plate elements under uniform compression (2). Previous research on lower strength steels has based the geometry of the plate elements on the criterion that the shape must undergo a strain at least equal to the strain-hardening strain without their buckling locally (5). The relevant formulas have been extended to include A572 (Grade 65) steel. Using these formulas and assuming $\sigma_y = 65$ ksi, $E_{st} = 600$ ksi, Poisson's ratio $\nu = 0.3$ and $E = 29,000$ ksi, the required flange slenderness ratio b/t is 11.8 and the web slenderness ratio d/w is 30.6. For the first test, a W16 x 71 shape was selected since its listed properties $b/t = 10.75$, $d/w = 33.2$ are fairly close to the requirements. The

actual ratios were 10.72 and 32.50 respectively. Web buckling was, therefore, anticipated to precede flange buckling.

The test results are shown in Fig. 5. The web buckled at a strain of 0.0073 in/in, followed almost immediately by flange buckling at a strain of 0.0079 in/in. These strains are much lower than ϵ_{st} in tension (0.0186 in/in) but close to ϵ_{st} in compression (0.0086 in/in). However, the load continued to be sustained until the strain reached 0.038 in/in.

Results of two other tests on modified W10 x 54 shapes are shown in Fig. 6. The flanges were machined down to yield b/t ratios of 11.8 and 13.3 for the two tests, while the web ratio d/w was maintained at 27.5. In the test with $b/t = 11.8$, the flanges buckled at a strain of 0.010 in/in and the webs at 0.015 in/in. Strain-hardening was evident later ($E_{st} = 950$ ksi) and the load began to drop off past the strain of 0.025 in/in. The third test with $b/t = 13.3$ showed nearly the same trends. Web buckling began at 0.006 in/in followed by flange buckling at 0.007 in/in with other details identical.

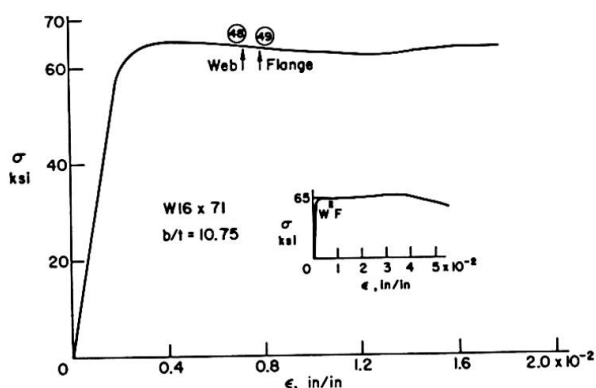


FIG. 5 STRESS-STRAIN CURVE FROM STUB COLUMN TEST - W16 x 71 SHAPE

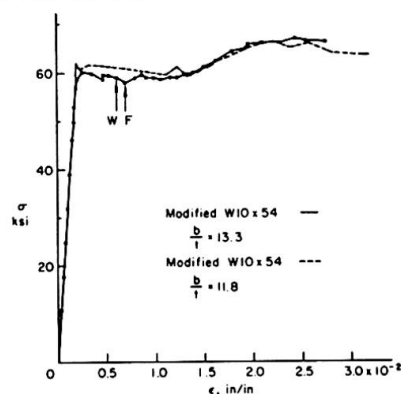


FIG. 6 STRESS-STRAIN CURVE FROM STUB COLUMN TEST - W10 x 54 SHAPE

The results show that local buckling occurred in Grade 65 steels at a strain smaller than that predicted by the theories developed for lower strength steels. Buckling, however, did not precipitate failure and resulting reduction in strength.

7. Beam Tests

Two beams fabricated from a length of W12 x 19 shape were tested, one under moment gradient and the other under uniform moment. Details are given elsewhere (6). Available theories indicate that the slenderness ratios b/t and d/w should be limited to 11.2 and 52.1, respectively, for $\sigma_y = 65$ ksi and $E_{st} = 600$ ksi. The W12 x 19 shape is one of the few having nearly these same ratios.

The beam under moment gradient had a simply supported span of 10'-5" and was loaded at the center. Lateral braces were provided at midspan, supports and at 37.5" on either side of midspan, as against the requirement of 46 ry or 38.5" according to available theories (7).

The non-dimensionalized moment M/M_p against midspan deflection δ/δ_p is given in Fig. 7. The terms M and δ are the moments and deflections, M_p is the theoretical plastic moment, and δ_p is the deflection at $M = M_p$, assuming ideal elastic behavior. Strain-hardening setting in soon after the plastic moment was reached at the center. Local buckling in the compression flange near midspan was visible at load No. 9. The compression flange also displaced laterally at load No. 13.

The rotation capacity of a beam is usually defined as $R = (\theta/\theta_p) - 1$ where θ is the sum of the end rotations at which the moment drops below $0.95 M_p$ and θ_p is the rotation at $M = M_p$. The R value is 3.1 in this test. A precise comparison of R with those obtained in other tests (for lower strength steels) is difficult, since different shapes and unbraced spans have been used. However, it can be said that the rotation capacity of Grade 65 steel beam is less than that for other beams.

The beam under uniform moment was loaded at quarter points over a simple span 15' long. Lateral braces were spaced, in close accordance with present theories (8), at load points, supports and approximately 13" apart between load points. Outside the uniform moment region, two braces were used, 37.5" from each load.

The results are shown in Fig. 8. The discontinuity of the curve between load Nos. 6 and 11 is due to a slip in a lateral brace and subsequent repair. Local buckling was visible at load No. 15 and the compression flange began to deflect laterally. At load No. 16, the lateral deflection was about 0.6 in. Unloading was caused by severe lateral buckling as a result of local buckling of the compression flange. The computed rotation capacity R in this test was 4.8, a value smaller than in comparable structures of lower strength steels.

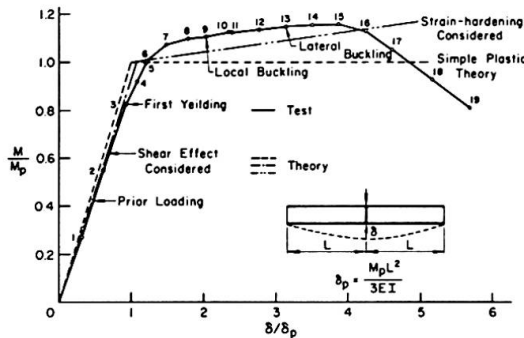


FIG. 7 BEAM UNDER MOMENT GRADIENT

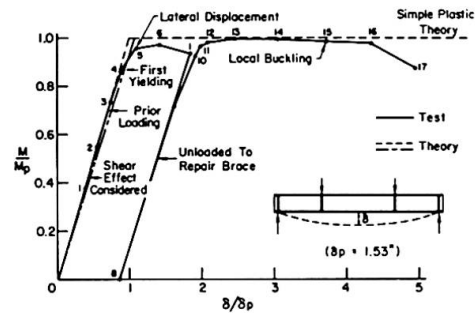


FIG. 8 BEAM UNDER UNIFORM MOMENT

8. Conclusions

A572 (Grade 65) steel exhibits mechanical properties in the inelastic region similar to those of structural carbon steel. The use of E_{st2} for strain-hardening modulus represents a new approach to obtain a more realistic, as well as conservative, value of this property for use in situations where the material is strained into the strain-hardening range. The value of E_{st} in compression is higher than in tension. Since buckling phenomena are associated with compression, a compression test appears to be the appropriate way of obtaining this modulus.

Residual stresses in shapes of higher strength steels are nearly the same in magnitude as in lower strength steels, and are thus independent of yield stress level. Hence, the influence of residual stresses decreases with increase in yield stress.

It was possible to extend the available theories developed for local and lateral buckling to Grade 65 steel although the assumptions of the theory are not fully borne out. This is because the post buckling strength of Grade 65 steel is considerable and reliable to the extent that it offsets any loss of strength as a consequence of premature buckling. Reference 9 contains the design recommendations developed for structures made of this steel.

References

1. Desai, S.
MECHANICAL PROPERTIES OF ASTM A572 GRADE 65 STEEL, Fritz Engineering Laboratory Report No. 343.2, Lehigh University, 1969
2. CRC
STUB COLUMN TEST PROCEDURE, CRC Technical Memorandum No. 3, 1961
3. Huber, A. W.
COMPRESSIVE PROPERTIES OF ROLLED STRUCTURAL STEEL, Fritz Engineering Laboratory Report No. 220A.1, Lehigh University, 1951
4. Huber, A. W. and Beedle, L. S.
RESIDUAL STRESS AND THE COMPRESSIVE STRENGTH OF STEEL, Welding Journal, 33(12) Research Suppl., 589-s, (1954)
5. Haaijer, G. and Thurlimann, B.
ON INELASTIC BUCKLING IN STEEL, Trans. ASCE, 125 (I), p. 308, (1960)
6. Kim, S. W.
EXPERIMENTS ON A512 GRADE 65 STEEL BEAMS, Fritz Engineering Laboratory Report No. 343.4, Lehigh University, 1970
7. Lay, M. G. and Galambos, T. V.
INELASTIC STEEL BEAMS UNDER MOMENT GRADIENT, Proc. ASCE, 93(ST1), (1967)
8. Lay, M. S. and Galambos, T. V.
INELASTIC STEEL BEAMS UNDER UNIFORM MOMENT, Proc. ASCE, 91(ST6), (1965)
9. ASCE-WRC Joint Committee
PLASTIC DESIGN IN STEEL -- A GUIDE AND COMMENTARY, ASCE Manual No. 41, 2nd edition, 1971

SUMMARY

The results of a study of the mechanical properties of ASTM A572 (Grade 65) steel and of the behaviour of simple structures made of this steel are presented. A new approach to define strain-hardening modulus is proposed. This modulus is significantly higher when it is determined from a compression test than from a tension test. Results of experiments on stub columns and beams show substantial post-buckling strength in the inelastic range.

RESUME

Les résultats d'une étude sur les propriétés mécaniques de l'acier désigné par ASTM A572 (grade 65) et sur le comportement de structures simples construites avec cet acier sont présentés. Une nouvelle méthode pour définir le module d'écrouissage est proposée. Ce module déterminé par des essais de compression est nettement plus grand que celui obtenu par des essais de traction. Les résultats des essais sur des colonnes courtes et sur des poutres indiquent que la résistance au flambage est importante dans la région inélastique.

ZUSAMMENFASSUNG

Die Ergebnisse eines Studiums über mechanische Eigenschaften des ASTM A572 (Grad 65) Stahles und das Verhalten der einfachen Konstruktionen aus diesem Stahl beschrieben. Es wurde ein neuer Versuch zur Definition des Verformungsmoduls dieses Stahles im Verfestigungsbereich vorgeschlagen. Dieser Modul ist wesentlich höher, wenn er aus Druckproben, jedoch nicht aus Zugproben bestimmt wird. Die Ergebnisse der Untersuchungen an kurzen Säulen und Balken haben gezeigt, dass der Stahl wesentliche überkritische Reserven im nichtelastischen Bereich aufweist.

Deformation Capacity of High-Strength Steel Members

Capacité de déformation d'éléments en acier à haute résistance

Verformungsfähigkeit von Gliedern aus hochfestem Stahl

<p>TOSHIRO SUZUKI Associate Professor, Dr. of Eng. Tokyo Institute of Technology Tokyo, Japan</p>	<p>TETSURO ONO Assistant, Dr. of Eng. Tokyo Institute of Technology Tokyo, Japan</p>
--	---

§1. INTRODUCTION

As large sized steel structures have been developed, high-strength steels having high yield stress level have attracted special interest recently. In this situation, it is becoming to be common to apply high-strength steel on the simple plastic design of structures. On the simple plastic design method, the steel structures must be able to maintain through a sufficient inelastic rotation without a decrease of moment capacity at each plastic hinge to allow the formation of a failure mechanism. Then, the deformation capacity of members comes up as an important problems. Therefore, there are many difficult problems in using high-strength steel which is less ductile than that of low-alloy steels. There are, however, few reports on high-strength steels concerning the simple plastic design of structures, and not enough of the necessary basic data.

The objectives of this paper are to explain the plastic behavior of high-strength steel members, and to determine quantitatively the relationship between the rotation capacity and the material properties of steels.

§2. OUTLINE OF EXPERIMENTS

2.1 EXPERIMENTS

Experiments are made to explain plastic behavior and deformation capacity of beams and beam-column. Test specimens of beams are built-up H-250×125×12×12 and test specimens of beam-columns are built-up H-150×150×9×9. The kinds of steel used in this experiments are low-alloy steels (SM-41, SM-50) and high-strength steels (HT-60, HT-80). The loading conditions of beams are a uniform moment and a moment gradient, and that of beam-columns are axial load and one end bending moment. In addition to using four kinds of steels, bracing spaces and axial forces are varied, in order to investigate their influences on the rotation capacity of these steel members.

2.2 MATERIAL PROPERTIES

The material properties of each steels are determined by tension tests and stub column tests with wide-flange shape. Yield stress level of high-strength steel has higher level, comparing low-alloy steel. Yield stress level of SM-41

is evaluated 3.24t/cm^2 , and that of HT-80 is evaluated 8.80t/cm^2 . The yield plateau length is short and the stress strain curve of HT-80 shows the stiff bi-linear material. The strain hardening modulus E_{st} is smaller than that of SM-41. Additionally, the yield ratio and elongation of the material are small. These results of each materials are showed in Table-1. The ductilities of material of high-strength steel are small as is obvious from Table-1. There are many difficult problems in applying high-strength steel on the plastic design for steel frames.

§3. EXPERIMENTAL RESULTS

3.1 LOAD-DEFLECTION CURVES

Fig. 1 ~ 3 show the experimental load-deflection curves. Moments and rotation angles have been nondimensionalized with full-plastic moment M_p and rotation angle θ_{pc} are used. Fig. 1 shows the load-deflection curves of beams under uniform moment. Moment reaches at full-plastic moment. Except HT-80, moment remains at near-constant value M_p and the in-plane deformations increase. This plastic behaviors are not influenced with the kinds of steel. Fig. 3 shows the load deflection curves of beams under moment gradient. These plastic behaviors are different from the beams under uniform moment. The plastic behaviors are effected with the strain hardening modulus and the plastic plateau length of material. Moments increase exceeding full plastic moment. In general, the strain hardening modulus has effects upon the rigidity of members after yielding. If the plastic plateau length is small, the effects of strain hardening modulus on plastic behaviors are remarkable. As the plastic plateau length decreases, the deformations of members at the same moment level are small. Fig. 4 shows the load deflection curves of beam-columns. In this case, the plastic behaviors are similar to that of beams under moment gradient.

3.2 LATERAL BUCKLING AND LOCAL BUCKLING

Fig. 4 ~ 6 show the strain distributions as the moments decrease due to local or lateral buckling. Fig. 4 shows the strain distributions along the axis of members at two points of M_p and the decrease of moment. When moments reach at M_p , the strain distributions are not uniform along the axis of members. The strain distribution of HT-80 are uniform and the level of strain is about the strain hardening level ϵ_{st} . Because the strain hardening modulus is small, the moment decreases rapidly. In the case of beams under uniform moment, the main cause of decrease of moment is the increase of torsional deformation. Fig. 5 shows the strain distributions of beams under moment gradient. The distributions are different from that of beams under uniform moment. On high-strength steel, the yield length is shorter than that of low-alloy steel and the gradient of strain distributions is large. On the beams under moment gradient, the local buckling causes the dropping of the applied load. Fig. 6 shows the curvature distributions along the axis of beam-columns and the strain distribution at the decrease of moment. Maximum curvature point moves to center from the end of span as the axial force increases. The behaviors at the decrease of moment are different each other due to the point of maximum moment. When the maximum moment occurs at the end of the beam-columns, strain distributions are uniform and deformations of out of plane are not recognized and the beam-columns have enough deformation capacity. These results show that the plastic behaviors of the beam-columns are same as the beam under moment gradient.

3.3 RELATION OF DEFORMATION CAPACITY AND MATERIAL PROPERTY

The deformation capacity of steel member is influenced with the material properties. Fig. 7 and 8 show the rotation capacity and slenderness ratio relationships of beam. It is clearly that each rotation capacities are different due to the material properties. In Fig. 7 and 8, the curves show the following equations.⁹ These equation are obtained from the analysis assuming two models.

Two models are based on the following ideas that are obtained from the experimental behavior. The lateral buckling and local buckling determine the limit of the deformation capacity.

Under uniform moment

$$R = K_1 \frac{1}{\lambda_y^2} (\sigma_y / \sigma_y)^2 \sqrt{\frac{B}{H}} \quad (1)$$

Under moment gradient

$$R = K_2 \frac{1}{\lambda_y^2} \rho (\sigma_y / \sigma_y) \left(\frac{t_f}{B} \right) \quad (2)$$

Fig. 9 shows the load-deflection curves of beam-columns which have same slenderness ratio ($\lambda_x=30$) and various axial force. Fig. 10 shows the relations of the rotations capacity and axial force with the slenderness ratio as a parameter. The curves in this figure are obtained from the numerical analysis according to the finite element method. Fig. 1 shows the critical slenderness ratio of beam-columns and experimental results. The rotation capacity of beam-columns is influenced with the axial force, the slenderness ratio and material properties. Especially, the deformation capacity of beam-columns is influenced more significantly with material. High-strength steel beam-columns (HT-60, HT-80) have few the rotation capacity. The curves in this figure show the critical slenderness ratio of beam-columns having enough rotation capacity. The thick solid line shows the critical value which can ensure the rotation capacity above $R=3$ due to the numerical analytical results. This result is agreement with the experimental results. Specification of AIJ is loose in order to have enough rotation capacity. From these results, the following critical slenderness ratio that is proposed by Lay, M.G.⁶ is equivalent to the experimental results.

$$P/P_y = \frac{1 - \bar{\lambda}}{1 + \bar{\lambda}} \quad (3)$$

§4. CONCLUSION

In this paper, the deformation capacity of steel members is explained by the experiment and numerical and theoretical analysis. In general, high-strength steel is seemed to be disadvantageous applying on the simple plastic design of steel structures which requires the enough rotation capacity. Especially, it is worth noting that HT-80 having the stiff bi-linear material curve used in this experiments has few deformation capacity. The rotation capacity is directly influenced by the value of yield stress, the plastic plateau length and the strain hardening modulus. Therefore, we concluded that the effective factors can be represented only by the ratio of yield stress. The rotation capacity is proportional to the square of the reciprocal ratio of yield stress in the case of uniform moment, and to the reciprocal ratio of that in the case of moment gradient. On the beam-columns, the redundant of rotation capacity is remarkable due to the material properties.

ACKNOWLEDGEMENT

In writing this paper the authors are grateful to Sumitomo Metal Industries, Ltd. for providing the test specimens of high-strength steel. Especially, the authors wish to thank Mr. Y. Nishida and Mr. M. Kato of Sumitomo Metal Industries, Ltd..

Table 1 Material Property

STEEL*	THICK- NESS (mm)	σ_y (t/cm ²)	σ_u (t/cm ²)	ϵ_y ($\times 10^{-3}$)	S (ϵ/ϵ_y)	$E \times 10^6$ (t/cm ²)	E_{st} (t/cm ²)	σ_u/σ_y	h (E/E_{st})	Elong. (%)
SM-41	12	3.24	4.76	1521.	13.8	2.13	47.0	1.47	45.3	28.5
SM-50	12	3.95	5.53	1855.	10.6	2.13	36.1	1.40	59.0	23.4
HT-60-1	12	5.78	6.78	2706.	6.78	2.14	31.0	1.17	69.0	26.6
(HT-60-2)	(12)	(5.45)	(6.65)	(2547.)	(5.89)	(2.14)	(36.4)	(1.20)	(58.0)	(30.7)
HT-80	12	8.80	9.39	4112.	1.00	2.14	15.0	1.07	142.7	24.4

*TEST COUPON DIMENSION (JIS Z 2201)

SM-41, SM-50.....No. 1 TEST COUPON

HT-60, HT-80.....No. 5 TEST COUPON

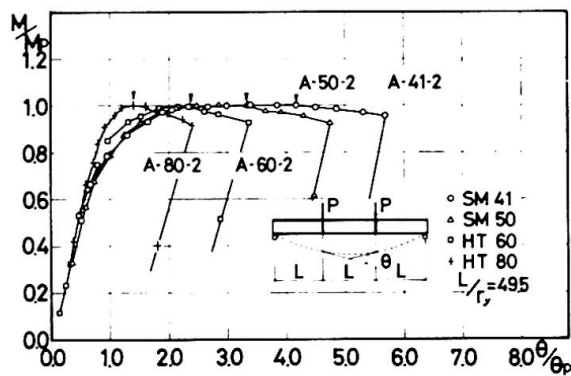


Fig.1 M-θ Relationships

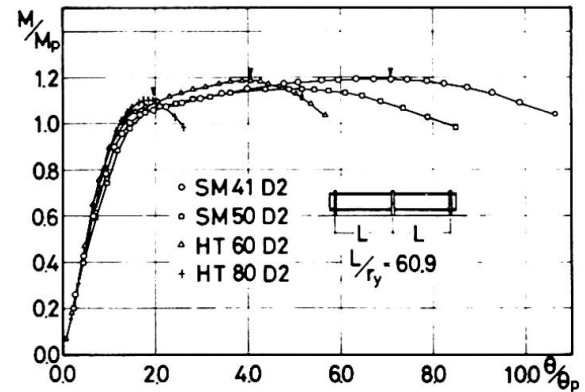


Fig.2 M-θ Relationships

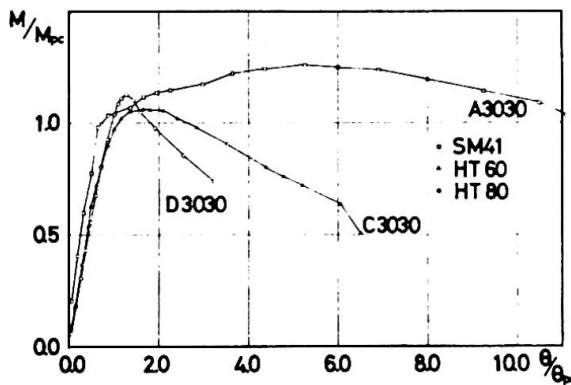


Fig.3 M-θ Relationships

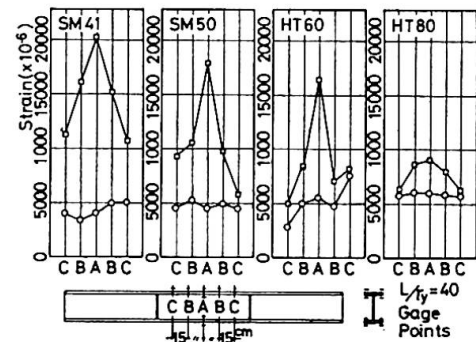


Fig.4 Strain Distribution

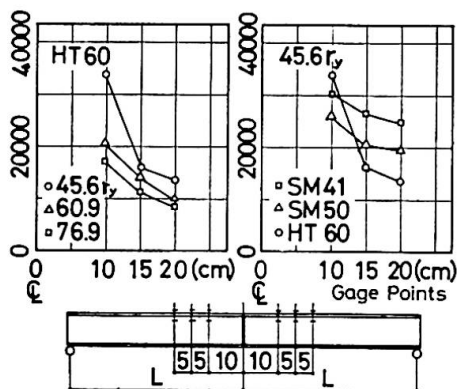


Fig.5 Strain Distributio

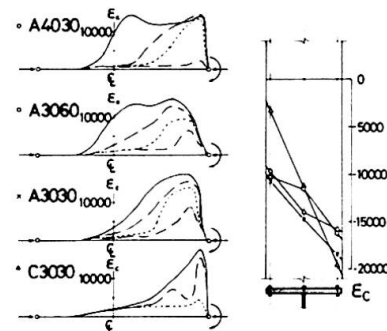


Fig.6 Strain Distributio

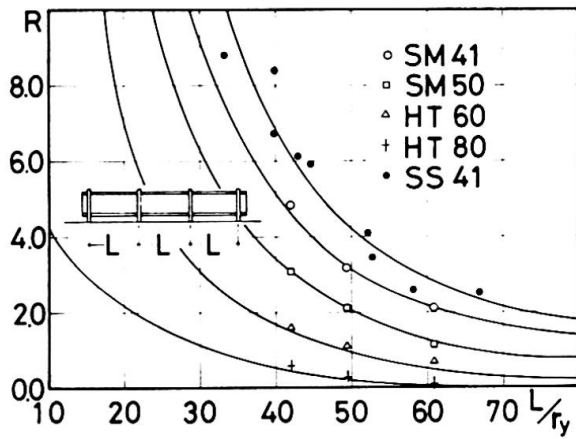


Fig.7 Rotation Capacity

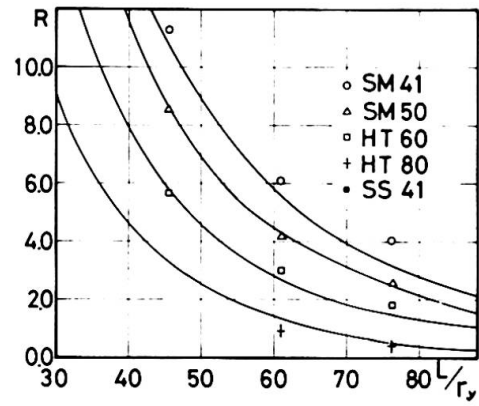


Fig.8 Rotation Capacity

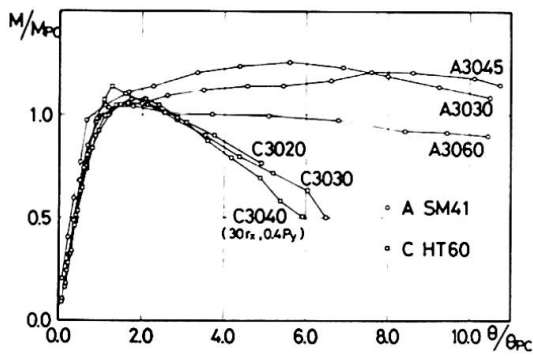


Fig.9 M-θ Relationships

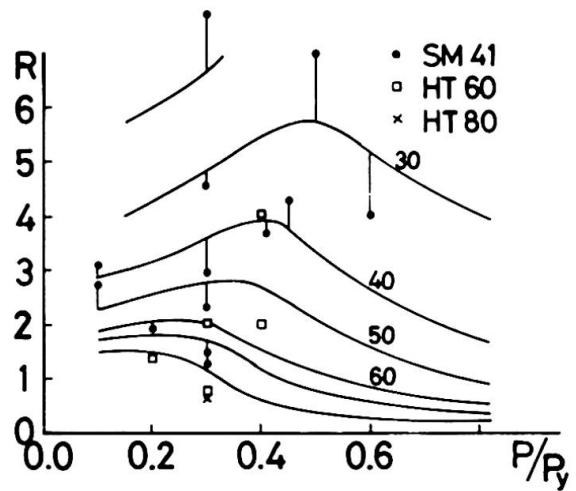


Fig.10 Rotation Capacity

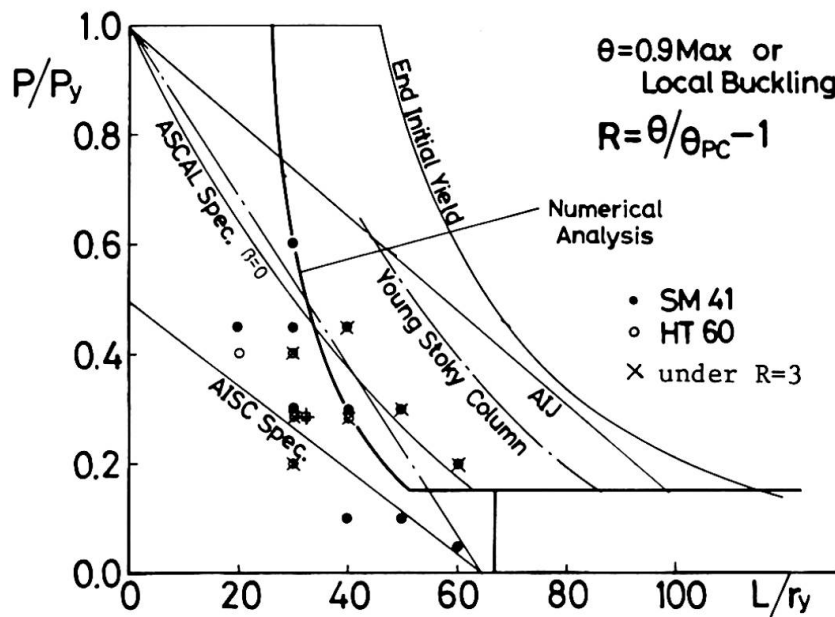


Fig.11 Critical Slenderness Ratio

REFERENCES

- 1) McDermott, J.F.; Plastic Bending of A514 Steel Beams, Journal of the Structural Div., Proc. ASCE, ST9, Sept. 1969
- 2) Plastic Design in Steel, A Guide and Commentary, 2nd Edition, ASCE, 1971
- 3) Adams, P. F., Lay, M. G. and Galambos, T. V.; Experimentary on High-Strength Steel Members, WRC Bulletin No. 110, Nov. 1965
- 4) Augusti, G.; Experimental Rotation Capacity of Steel Beam-Columns, Journal of the Structural Div., Proc. ASCE, ST6, Dec. 1964
- 5) Adams, P. F.; Plastic Design in High Strength Steel, Fritz Engineering Laboratory Report, No. 297, 19, May, 1966
- 6) Lay, M. G.; The Static Load-Deformation Behavior of Planner Steel Structures, Ph. D. Dissertation, Lehigh Univ., 1964
- 7) Suzuki, T. and Ono, T.; Experimental Study of the Inelastic Steel Beams (1), Trans. AIJ, No. 168, Feb. 1970
- 8) Suzuki, T. and Ono, T.; Experimental Study of the Inelastic Steel Beams (2), Trans. AIJ, No. 170, May, 1970
- 9) Suzuki, T. and Ono, T.; Experimental Study of the Plastic Design of High-Strength Steel Beams, Trans. AIJ, No. 219, May, 1974

SUMMARY

The plastic behaviour and the deformation capacity of high-strength steel members are discussed on the relation to the low-alloy steel members. High-strength steels seem to be disadvantageous applying on the simple plastic design of steel structures. Especially, it is worth noting that HT-80 used in this experiment has few deformation capacity. While the rotation capacity is directly influenced by the value of yield stress, plastic flow and strain hardening rigidity, we conclude that the effective factors can be represented only by the ratio of yield stress.

RESUME

Le comportement plastique et la capacité de déformation d'éléments en acier à haute résistance sont comparés avec ceux de l'acier doux. Il semble que les aciers à haute résistance sont désavantageux lors du calcul plastique simple de structures en acier. Il faut remarquer que l'acier HT-80 employé dans cette expérience a une faible capacité de déformation. La capacité de rotation d'éléments en acier est directement influencée par la valeur de l'effort à la limite d'écoulement, l'écoulement plastique, et le durcissement par déformation. D'autre part nous concluons que ces facteurs efficaces peuvent être représentés seulement par le rapport d'efforts à la limite d'écoulement.

ZUSAMMENFASSUNG

Plastische Verhalten und Verformungsfähigkeit von Gliedern aus hochfestem Stahl werden in Beziehung zu denselben von Gliedern aus Stahl St 37 diskutiert. Es scheint, dass hochfeste Stähle bei Anwendung der einfachen plastischen Berechnung von Stahlbauten nachteilig sind. Bemerkenswert ist, dass in diesem Experiment HT-80 eine geringe Verformungsfähigkeit zeigt. Die Rotationsfähigkeit von Gliedern aus Stahl werden unmittelbar durch die Höhe der Fließgrenze, die Fließverformung und die Steifigkeit im Verfestigungsbereich beeinflusst. Andererseits kommen wir zur Ueberzeugung, dass diese wirksamen Faktoren nur durch das Verhältnis der Fließgrenzen dargestellt werden können.

Lateral Buckling of Welded Beams and Girders in HT 80 Steel

Déversement de poutres soudées en acier HT 80

Kippen von geschweissten Balken aus HT 80 Stahl

YUHSI FUKUMOTO
Professor of Civil Engineering
Nagoya University
Nagoya, Japan

1. INTRODUCTION

Lateral instability of compression flange has been one of the important limit state criteria for the determination of the ultimate bending strength of flexural members when the compression flange is not restrained enough against lateral deflection. The author has shown the results of the investigation on the ultimate strength of beams with lateral bracing at the intermediate points and without any lateral supports in between^{1),2),3),4),5)} from theory and test.

This paper briefly describes the lateral buckling test³⁾ on welded beams and girders with steels of SM 50 and quenched and tempered HT 80 (nominal yield stresses $\sigma_y = 3200\text{kg/cm}^2$ and 7000kg/cm^2 , respectively), and the initial imperfections such as welding residual stresses and initial deformations are discussed with the test results. The comparisons are also made between theory and test.

2. THE TEST SPECIMEN

No lateral bracings are provided except at the both ends of the specimen where the loading beams with heavy box cross section are connected using high strength bolts. The end condition of the specimen is thus clamped laterally and torsionally at the both ends. The test setup is shown in Fig. 1.

The detailed nominal dimension of the beam-type specimens are given in Table 1(a). The beam types are of 25cm or 30cm in beam height with the span length ranging from 2.5m to 4.5m. Total number of beam specimens is thirty-six of which

SM 50 : twenty-one including nine annealed beams, and

HT 80 : fifteen including three annealed beams.

Table 1(b) shows for the plate girders of 80cm or 100cm in height with the span length ranging from 2.8m to 4.0m. Number of sub-panels in web is two for G-D and the others have three sub-panels.

The specimens are tested under uniform bending and under moment gradient with the end moment ratio of 0.5.

3. INITIAL IMPERFECTIONS

After the test specimen is set in the position for testing and just prior to loading, the initial imperfections are measured in flanges and web plates. Table 2 summarizes the maximum lateral deflections of the compression flange δ_u and tension flange δ_t at the span center. Effective length of the specimens against lateral buckling becomes $L_e = L/2$ (L =length of the specimen) under uniform bending since the clamped end condition is met at the connections of the specimens and the loading beams.

4. WELDING AND ANNEALING DATA

Welding data for HT 80 steel specimens are as follows ;

For beams : Manual welding with 5mm ϕ electrode (YAWATA L80). 180 - 230 amp. current and preheating at 120 $^{\circ}$ C.

For girders : Manual welding with 4mm ϕ electrode (KAWASAKI KS116, B-1). 165 - 175 amp. current and preheating at 120 $^{\circ}$ C.

Annealing conditions are set for relieving the welding residual stress as shown in Fig. 2.

5. THE TEST RESULTS

a) Tension Coupon Test

Test coupons with 20cm gage length for SM 50 and with 5cm gage length for HT 80 are cut out from the flange and web plates. The averaged values of static yield stress are listed below.

Beams { SM 50 : 3428 kg/cm 2
HT 80 : 7841 "

Girders { SM 50 : 3810 kg/cm 2 (8mm) and 3236 kg/cm 2 (10mm)
HT 80 : 7850 " (10mm) and 6610 " (6mm)

b) Lateral Buckling Test

Figs 3a and 3b show the load-deflection curves of a beam and a girder in HT 80, respectively, in which β = angle of rotation of the compression flange, u_1 and u_2 = lateral deflection of lower and upper flanges and v = vertical deflection at the span center. At the early stage of loading, the lateral and torsional deformations of the girder flanges are observed together with the buckled patterns in each web panel. Lateral deflection of the compression flange at failure is influenced considerably by the direction of the buckled deformation of the web in bending.

A summary of test results with the reference loads is listed in Table 3.

Fig. 4 shows a presentation of the test points plotted on the $\sigma_{cr} - (r_x/r_y)(L/d)$ axes³⁾, in which r_x and r_y are the radii of gyration of cross section about x and y axes, respectively and d = the beam height. The test points for HT 80 indicate less scatter and the reduction of lateral buckling strength becomes less for HT 80 specimens compared with SM 50 specimens in the inelastic range.

Fig. 5 shows another presentation of the test points plotted for beam-type specimens on the $\sigma_{cr}/\sigma_y - (L/r_y)/(L/r_y)_{elastic}$ axes. Non-dimensionalized slenderness ratio λ is taken in the abscissa whereas $(L/r_y)_{elastic}$ is the slenderness ratio at which the elastic lateral buckling stress reaches to the yield point, that is, $\sigma_{cr} = \sigma_y$. The maximum experimental moments M_u are non-dimensionalized by the yield moment M_y . In order to clarify the effect of residual stress distributions on the lateral buckling strength of steel beams, the comparisons are made between the annealed beams and the as-weld beams having the same sizes. Twelve pairs of specimens are tested and by taking the strength ratios $M_{annealed}/M_{as-weld}$ for each pair, it is obtained that the average strength gains are of 11% for annealed beams compared to the as-weld beams for SM 50 and 6% for HT 80 steel. It may be concluded that the welding residual stress distributions may reduce the lateral buckling strength for about 11% average for SM 50 and 6% average for HT 80 against the beams without residual stresses. Experimental findings may prove that the residual stress effect upon the lateral buckling strength becomes less with the higher yield strength steel.

6. COMPARISONS OF THEORY AND TEST

a) Inelastic Lateral Buckling Strength

Inelastic lateral buckling strength under uniform moment is determined for the arbitrary residual stress patterns using the numerical iteration technique for computing the cross sectional properties.^{5) 7)} In Table 4 the calculated ideal critical elastic moment M_E and inelastic moment M_{cr} for the two different residual stress patterns (A) and (B) are given for girder-type specimens. Fig. 6 shows the theoretical results using the residual stress patterns 1 and 2 ($\sigma_{rc} = 0.3\sigma_y$ inset in Fig. 6) are compared with the test points for the as-weld^{rc} and annealed A-type beams.³⁾

b) Ultimate Bending Strength

Since the inelastic lateral buckling resistance is furnished mostly by the compression flange, the lateral buckling strength becomes very close to that of a column whose effective cross section is composed of the compression flange and one-sixth of the web⁶⁾. In this analysis the ultimate bending strength of members with initial imperfections such as residual stresses and lateral deflection of the compression flange is determined by the beam-column concept using the numerical integration technique⁵⁾. The residual stress patterns used for this analysis is shown in Table 4 as patterns (C) and (D).

In Fig. 5 the ultimate bending strength curves obtained by the beam-column concept are given for the D-type and C-type beams with the initial lateral deflection $u_o = L/1000$ and with and without residual stress pattern (C). Ultimate bending strength curves for the residual stress patterns (C) with, $\sigma_{rc} = 0.3\sigma_y$ and initial lateral deflection $u_o = L/1000$ may explain the lower bound^{rc} estimate against the plotted test results. In table 4 the numerical results by the beam-column approach are also given for the plate girders G-A~G-G.

Table 1(a) Dimensions of test beams

Test Beams	Steel	d (mm)	b (mm)	t _w (mm)	t (mm)	L (mm)	End Moment Ratio	Remarks
A-1-0	S460A	250	100	6	8	3000	1.0	as-weld
A-1-1	S460A	250	100	6	8	3000	0.5	as-weld
A-1-2	S460A	250	100	6	8	4000	1.0	as-weld
A-2-0	S460A	250	100	6	8	4000	1.0	as-weld
A-2-1	S460A	250	100	6	8	4000	0.5	as-weld
A-2-2	S460A	250	100	6	8	4000	1.0	as-weld
A-3-0	S460A	250	100	6	8	4500	1.0	as-weld
A-3-1	S460A	250	100	6	8	4500	1.0	as-weld
A-3-2	S460A	250	100	6	8	4500	0.5	as-weld
B-1-0	S460A	250	130	6	8	3000	1.0	as-weld
B-1-1	S460A	250	130	6	8	3000	1.0	as-weld
B-2-0	S460A	250	130	6	8	4000	1.0	as-weld
B-2-1	S460A	250	130	6	8	4000	1.0	as-weld
B-3-0	S460A	250	130	6	8	4500	1.0	as-weld
B-3-1	S460A	250	130	6	8	4500	1.0	as-weld
C-1-0	S460A	300	100	6	8	3000	1.0	as-weld
C-1-1	S460A	300	100	6	8	3000	1.0	as-weld
C-2-0	S460A	300	100	6	8	4000	1.0	as-weld
C-2-1	S460A	300	100	6	8	4000	1.0	as-weld
C-3-0	S460A	300	100	6	8	4500	1.0	as-weld
C-3-1	S460A	300	100	6	8	4500	1.0	as-weld
D-1-0	HT80	250	100	7	10	2500	1.0	as-weld
D-1-1	HT80	250	100	7	10	2500	0.5	as-weld
D-2-0	HT80	250	100	7	10	3000	1.0	as-weld
D-2-1	HT80	250	100	7	10	3000	0.5	as-weld
D-2-2	HT80	250	100	7	10	3000	1.0	as-weld
D-3-0	HT80	250	100	7	10	3500	1.0	as-weld
D-3-1	HT80	250	100	7	10	3500	0.5	as-weld
D-3-2	HT80	250	100	7	10	3500	1.0	as-weld
E-1-0	HT80	250	130	7	10	2500	1.0	as-weld
E-2-0	HT80	250	130	7	10	3000	1.0	as-weld
E-3-0	HT80	250	130	7	10	3500	1.0	as-weld
F-1-0	HT80	300	100	7	10	2500	1.0	as-weld
F-2-0	HT80	300	100	7	10	3000	1.0	as-weld
F-3-0	HT80	300	100	7	10	3500	1.0	as-weld

d = beam height, b = flange width, t_w = flange thickness, t = web thickness, L = beam length

Table 1(b) Dimensions of test girders

Test Girders	Steel	d (mm)	b (mm)	t _w (mm)	t (mm)	L (mm)	End Moment Ratio
G-A	S460A	1000	130	6	10	4100	1.0
G-B	S460A	1000	130	6	8	4100	1.0
G-C	HT80	800	110	6	10	3300	1.0
G-D	HT80	800	110	6	10	2800	1.0
G-E	HT80	800	130	6	10	3300	1.0
G-F	HT80	800	130	6	10	2800	1.0
G-G	HT80	800	110	6	10	3300	1.0

Table 3 Summary of reference and experimental loads

Specimens	M _y (t-m)	M _p (t-m)	M _{max} (t-m)	e _{max} (kg/cm ²)	M _{max} /M _y
A-1-0	8.18	9.45	7.69	3218	0.94
A-1-1	8.18	9.45	7.00	2929	0.86
A-1-2	8.18	9.45	9.70	4059	1.19
A-2-0	8.18	9.45	7.94	3322	0.97
A-2-1	8.18	9.45	6.61	2766	0.81
A-2-2	8.18	9.45	8.42	3523	1.03
A-3-0	8.18	9.45	6.33	2649	0.77
A-3-1	8.18	9.45	5.75	2405	0.70
A-3-2	8.18	9.45	8.54	3573	1.04
B-1-0	9.47	10.78	9.40	3406	0.99
B-1-1	9.47	10.78	8.00	2899	0.84
B-2-0	9.47	10.78	8.60	3115	0.91
B-2-1	9.47	10.78	8.76	3174	0.93
B-3-0	9.47	10.78	9.28	3362	0.98
B-3-1	9.47	10.78	7.10	2572	0.75
C-1-0	10.41	12.16	7.58	2433	0.73
C-1-1	10.41	12.16	9.20	3025	0.88
C-2-0	10.41	12.16	8.04	2645	0.77
C-2-1	10.41	12.16	6.88	2263	0.66
C-3-0	10.41	12.16	7.48	2461	0.72
C-3-1	10.41	12.16	6.89	2266	0.66
D-1-0	22.53	26.08	21.16	7373	0.94
D-1-1	22.53	26.08	20.89	7279	0.93
D-1-2	22.53	26.08	27.90	9721	1.24
D-2-0	22.53	26.08	20.68	7206	0.92
D-2-1	22.53	26.08	18.54	6460	0.82
D-2-2	22.53	26.08	23.10	8049	1.03
D-3-0	22.53	26.08	19.21	6693	0.85
D-3-1	22.53	26.08	16.24	5659	0.72
D-3-2	22.53	26.08	21.84	7610	0.97
E-1-0	26.14	29.84	26.46	7946	1.01
E-2-0	26.14	29.84	24.42	7333	0.93
E-3-0	26.14	29.84	22.79	6844	0.87
F-1-0	28.68	33.50	26.32	7191	0.92
F-2-0	28.68	33.50	22.42	6126	0.78
F-3-0	28.68	33.50	20.78	5678	0.73
G-A	71.68	106.32	43.6	1968	0.61
G-B	72.31	93.74	41.0	2160	0.57
G-C	113.90	128.81	64.4	4438	0.57
G-D	113.90	128.81	83.4	5748	0.73
G-E	126.15	140.23	94.8	5899	0.75
G-F	126.15	140.23	105.1	6540	0.83
G-G	113.90	128.81	65.5	4514	0.58

M_y = Calculated Yield Moment

M_p = Calculated Plastic Moment

Table 2 Initial imperfections of flanges

Test Beams and Girders	Upper flange δ _u (mm)	Lower flange δ _l (mm)	δ _u /L	δ _l /L
A-1-0	0	0	0	0
A-1-1	1.5	0	1/1960	0
A-3-1	4.5	0	1/1000	0
B-1-0	3	8	1/990	1/370
B-2-0	0	2	0	1/1985
B-3-1	0	6	0	1/745
C-1-0	1.5	1.5	1/1970	1/1970
C-1-1	4.8	6.8	1/620	1/435
D-2-0	0	0	0	0
D-2-2	0	0	0	0
D-3-1	2.5	0	1/1400	0
D-3-2	1	0	1/3470	0
E-2-0	1	0	1/2960	0
E-3-0	2.5	0	1/1390	0
G-A	1	1.5	1/4100	1/2720
G-B	1	5	1/4100	1/820
G-C	1	2	1/3300	1/1650
G-D	3	3	1/940	1/940
G-E	0	0	0	0
G-F	2	0	1/1400	0
G-G	0	1	0	1/3300

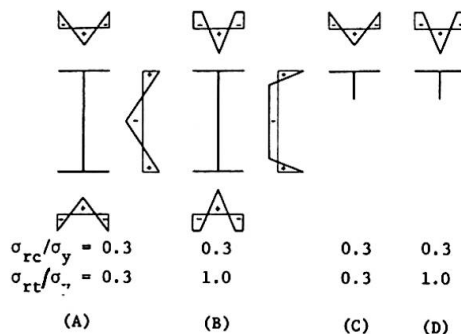
Table 4 Comparison of theory and test for girders

Test Girders	Experimental	Theoretical									
		Lateral Buckling Strength					Ultimate Bending Strength				
		Residual Stress Patterns					Residual Stress Patterns				
		(A)		(B)		(C)	(D)		(E)	(F)	
$M_{u,EB}$ (kN-m)	$M_{u,EB}$ (kN-m)	$M_{u,EB}$ (kN-m)	$M_{u,EB}$ (kN-m)	$M_{u,EB}$ (kN-m)	$M_{u,EB}$ (kN-m)	$M_{u,EB}$ (kN-m)	$M_{u,EB}$ (kN-m)	$M_{u,EB}$ (kN-m)	$M_{u,EB}$ (kN-m)	$M_{u,EB}$ (kN-m)	
G-A	43.6	87.55	56.63	1.30	49.82	1.14	48.75*	1.12	44.38	1.02	
G-B	41.0	33.32	31.32	1.25	46.99	1.15	41.09	1.00	38.17	0.93	
G-C	64.4	69.33	68.75	1.07	68.25	1.06	53.27	0.83	51.20	0.80	
G-D	83.4	96.06	83.60	1.00	75.87	0.91	54.29	0.85	52.45	0.83	
G-E	94.8	114.16	93.83	0.990	81.39	0.86	78.46	0.95	74.93	0.90	
G-F	105.1	137.99	99.31	0.93	82.40	0.78	90.54	0.96	85.43	0.90	
G-G	65.3	67.60	67.10	1.02	66.62	1.02	68.79	0.73	64.93	0.71	
							76.79	0.94	73.66	0.91	
							48.85	0.74	47.72	0.73	

* Upper line is for δ_u indicated in Table 2

** Lower line is for infinitesimal small u₀ as u₀ = L_e/10,000

Assumed Residual Stress Patterns



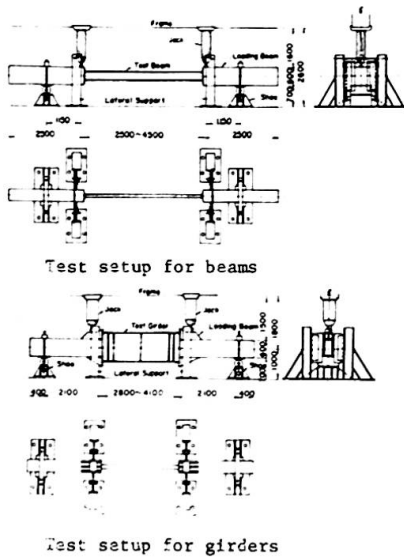


Fig. 1

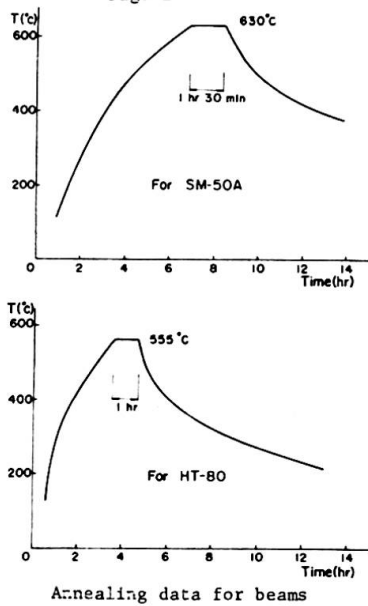


Fig. 2

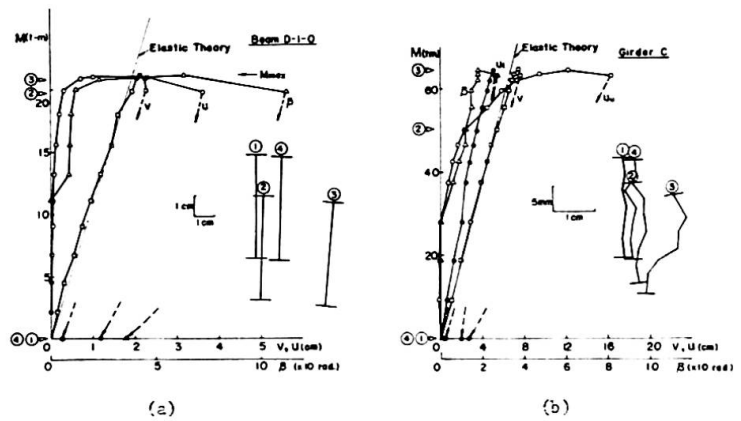


Fig. 3

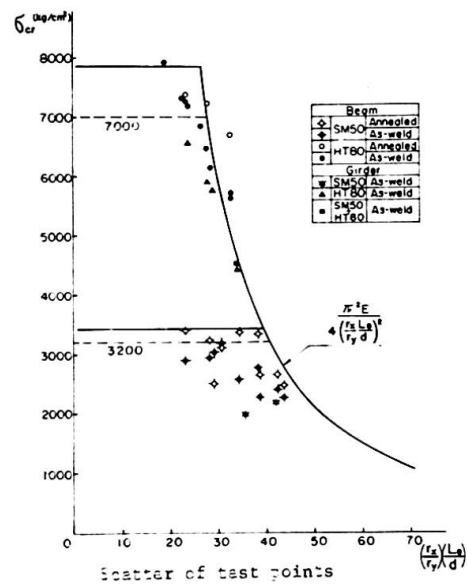


Fig. 4

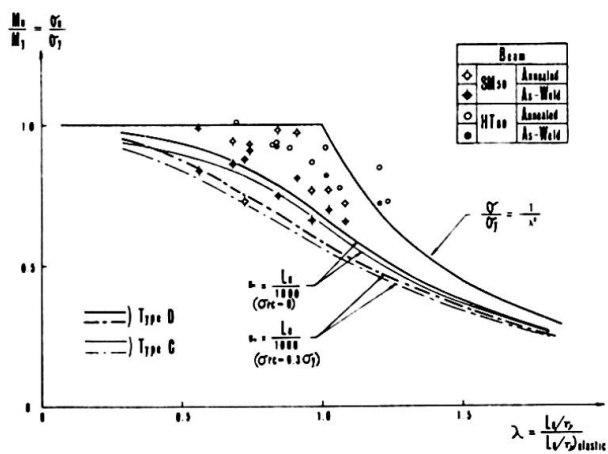


Fig. 5

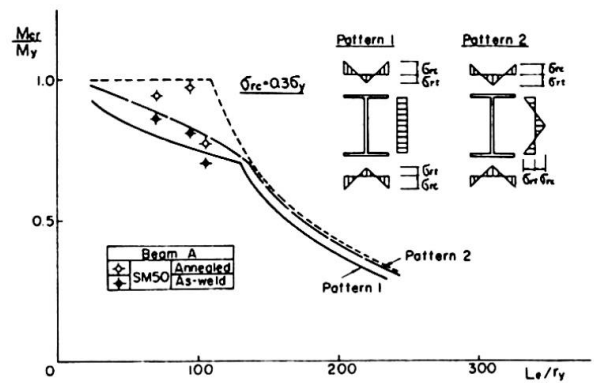


Fig. 6

REFERENCES

- 1) Fukumoto, Y. and Kubo, M., "Lateral Buckling Strength of Girders with Bracing Systems", Preliminary Report, 9th Congress IABSE, Amsterdam, 1972.
- 2) Fukumoto, Y. and Kubo, M., "Lateral Buckling of Braced Beams", Trans. of Architectural Institute of Japan, No. 206, April, 1973.
- 3) Fukumoto, Y., Fujiwara, M. and Watanabe, N., "Inelastic Lateral Buckling Tests on Welded Beams and Girders", Proc. of Japan Society of Civil Engineers, No. 189, May, 1971.
- 4) Fukumoto, Y., et al, "Research Works on Ultimate Strength of Plate Girders, and Japanese Provisions on Plate Girder Design, "Design of Plate and Box Girders for Ultimate Strength", IABSE Colloquium, Proc. Volume II, London, 1971.
- 5) Fukumoto, Y. and Kubo, M., "Ultimate Bending Strength of Plate Girders with Longitudinal Stiffeners failed by Lateral Instability", to be published from Der Stahlbau.
- 6) Basler, K. and Thürlimann, B., "Strength of Plate Girders in Bending", Journal of Structural Division, ASCE Vol. 87, No. ST 6, August, 1961.
- 7) Yoshida, H., "Lateral Buckling Strength of Plate Girders", Publications, IABSE Vol. 35-II, 1975.

SUMMARY

This report presents the results of an extensive experimental investigation into the behaviour and strength of flexural members with high strength steels which are failed by lateral buckling. A total thirty-six beam-type and seven girder-type members is tested under uniform moment and moment gradient. Test results of as-weld and annealed specimens are compared with the inelastic lateral buckling theory with the specified residual stress patterns and also with the beam-column approach to ultimate bending strength using the effective compressive section with initial imperfections.

RESUME

Ce rapport présente les résultats d'essais détaillés sur le comportement de la résistance d'éléments en acier à haute résistance soumis à la flexion, et qui ont été détruits par déversement. Les essais de spécimens soudés et recuits ont été comparés selon la théorie du déversement, en fonction des contraintes résiduelles, ainsi que selon l'approche "poutres-colonnes" pour le moment fléchissant de rupture, considérant la section effectivement comprimée avec des imperfections initiales.

ZUSAMMENFASSUNG

Dieser Bericht enthält die Resultate einer ausführlichen experimentellen Untersuchung über das Verhalten und die Tragfähigkeit von Biegeträgern aus hochfesten Stählen, die durch Kippen zerstört wurden. Eine Gesamtheit von 36 Trägertypen und 7 Balkenträgern wurden unter konstanten, linear verlaufenden Biegemomenten getestet. Testresultate von geschweissten und spannungsarm geglühten Proben wurden mit der unelastischen Kipptheorie und den bezeichnenden Eigenspannungsverteilungen und ebenso mit einer Näherungsuntersuchung als exzentrischem Knicken verglichen, indem die effektiv zusammendrückenden Abschnitte mit anfänglichen Imperfektionen verwendet werden.

Study on Hybrid Girders

Etude de poutres hybrides

Studien über hybride Tragbalken

TETSUO KUNIHIRO SHOICHI SAEKI KEIICHI INOUE

Public Works Research Institute

Ministry of Construction

Tokyo, Japan

Introduction

Different from the universally used homogeneous girders (girders made homogeneously with the same grades of steel), the hybrid girder is made of different grades of steel in its upper and lower flanges and web. Cost of materials for a hybrid girder can be reduced by using high-strength steel for upper and lower flanges which are effective for the flexural rigidity and using mild steel for the web. It has been made known that the hybrid girder is by no means inferior in bending strength to the homogeneous girder in which high-strength steel is used for both flanges and web of the same section, and that by using mild steel for the web the hybrid girder can be made economical.

Provisions on the design for hybrid girders have already been enforced in the U.S.A. In Japan provisions on this kind of girders will be provided for in the specifications for highway bridges in the near future.

Introduced hereunder are the results of researches continuously conducted on this kind of girders by the Public Works Research Institute, Ministry of Construction.

1. Economical Efficiency of Hybrid Girders

Haaijer has published his thesis on the economical efficiency of the hybrid girders. Referring to this thesis, the ratio of cost of a hybrid girder to that of homogeneous girder (C_h/C_o) is expressed by the following formula in case where the hybrid girder is fitted with symmetrically arranged upper and lower flanges having same bending strength (M_p).

$$\frac{C_h}{C_o} = \eta \left(\frac{h_{wy}}{h_{ow}} \right)^2 \cdot \frac{2\beta - \gamma}{\beta} \quad (1)$$

where, $\frac{h_{wy}}{h_{ow}} = \left(\frac{\psi \gamma}{2\beta - \gamma} \right)^{1/3}$

$\psi = \frac{\text{Web yield stress of homogeneous girder}}{\text{Web yield stress of hybrid girder}}$

$\eta = \frac{\text{Unit price of steel grade for the web of hybrid girder}}{\text{Unit price of steel grade for the web of homogeneous girder}}$

$\beta = \frac{\text{Flange yield stress of hybrid girder}}{\text{Web yield stress of hybrid girder}}$

$\gamma = \frac{\text{Unit price of steel grade for the flange of hybrid girder}}{\text{Unit price of steel grade for the Web of hybrid girder}}$

Using the above formulae and unit prices in 1971 and in 1975, cost was compared between the hybrid girders in which steel grades of SM41, SM50 were used for the webs and SM50Y, SM58, HT70, HT80 (Table 1) for flanges and the homogeneous girders. The results are shown in Fig. 1. The results show that a maximum of 13% cost down can be obtained with the steel up to SM58 as provided for in the specifications for highway bridges by 1971's prices, but that the hybrid girders don't make

Table 1. Mechanical Property of Steel

Grades of Steel	Yielding point (kg/mm)	Tensile strength (kg/mm)
SS 41	24	41
SM 50	32	50
SM 50 Y	36	50
SM 58	46	58
HT 70	56	70
HT 80	70	80

economical efficiency due to the relative reduction of prices of SM50Y and SM58 in 1975.

As steel products under the grade of SM58 is so popular that the unit prices of these steels have been reduced in Japan, the hybrid girder is not superior economically, but when unit price of ultra high strength steel as HT80 is reduced in future, this type of girder will be superior economically.

Apart from the foregoing, economical efficiency is under study as to the girders made under the standards (draft) drawn up by our research institute for the hybrid plate girders.

2. Design Problems in Hybrid Girders

As mentioned already, different grades of steel are used respectively for the flanges and webs of hybrid girders. Therefore, in the case of the hybrid girders, the webs start yielding before the flanges do it, while in the case of the homogeneous girders yielding stresses both in webs and flanges are equal. This means that when the flange of the hybrid girder starts yielding, not a small part of the web has already yielded. Thus, under a load for which the flanges are still in elastic region, part of the web has already yielded and thereby gives rise to problems on the following 4 points as viewed comparatively with the homogeneous girder.

- (i) Bending characteristics
- (ii) Buckling
- (iii) Fatigue strength
- (iv) Design on field joint

With reference to the bending characteristics, buckling of compression flanges and fatigue strength, results of experiments carried out by the Public Works Research Institute will be explained in paragraphs 3, 4 and 5.

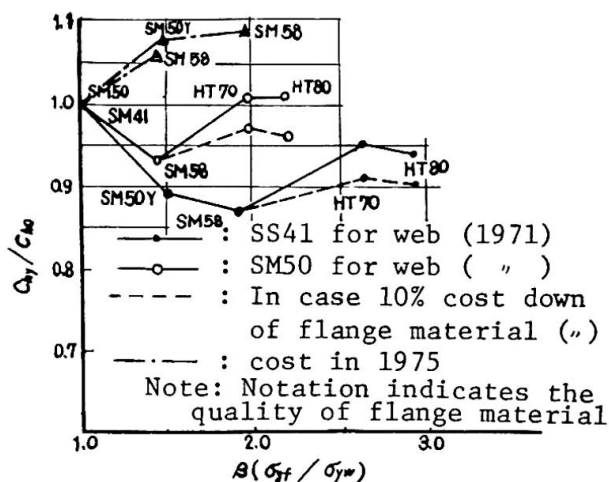
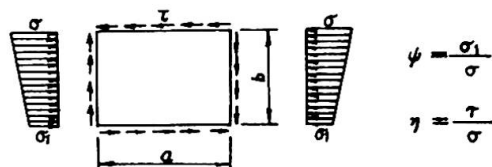
As regards another problem of web buckling, the minimum thickness of the web plate, that is subject to bending and shearing, is determined from the following formula in the existing highway bridge specifications.

$$\left(\frac{b}{t}\right)^2 \geq \frac{V_B \sigma_c}{(1378 K)^2} \left\{ \frac{1+\psi}{4k_\sigma} + \sqrt{\left(\frac{3-\psi}{4k_\sigma}\right)^2 + \left(\frac{n}{k_\tau}\right)^2} \right\}$$

V_B : Buckling safety factor $1.25 + (0.30 + 0.15\psi)e^{-4.3n} < 1.25$
 K = $0.09 - 0.10\psi$
 k_σ : Buckling coefficient for fiber stress intensity
 k_τ : Buckling coefficient for shearing stress intensity
 μ : Poisson's ratio

If this concept can be extended, the normal value of the minimum plate thickness becomes $1/\sqrt{R}$ times thicker. In this respect, experimental proving may be necessary. Here, R is the reduction factor of the allowable stress adopted in the AASHTO's specifications for highway bridges or the ratio between the stress obtained from the section modulus calculated for the homogeneous girder and the actual stress of the hybrid girder. This ratio can be expressed by the following formula if the flange thickness is disregarded.

$$R = 1 - \frac{\beta\psi(1-\alpha^2)(3-\psi+\psi\alpha)}{6+\beta\psi(3-\psi)}, \quad \alpha = \frac{\sigma_{yw}}{\sigma_{yf}}, \quad \beta = \frac{2A_w}{A_f}, \quad \psi = \frac{\bar{x}}{h}$$

Fig. 1 Relations between β and C_{hy}/C_{ho} 

In designing the field joints we are confronted with a problem of how to deal with the reduction of the axial force in the high strength bolts at the yielding part of the web. Our research institute has been doing the experiments thereof.

3. Experiments on Bending Characteristics of Hybrid Girders

Referring to the results of studies both at home and abroad on the plate girders, especially those for hybrid girders static load tests were conducted using a total of 8 specimens which were composed of 2 girders each of the following types 1 and 2 (shown in Fig. 3) and 2 girders each of the following modified girders of types 1 and 2 (shown in Fig. 4).

Type 1: A girder whose flanges were made of SM58 and web SS41 and the depth/thickness ratio (D/T) of the web was 160.

Type 2: A girder made of same construction but the depth/thickness ratio of the web was 200.

Modified girder: Above types 1 and 2 fitted with a slab to prevent local buckling of the compression flanges and transverse buckling of the girder.

Table 2 shows the moment inertia, section modulus and various load values for all girders. Fig. 5 shows the loading methods. The results of test on materials used are shown in Table 3. The load-deformation curves for all test specimens are shown in Fig. 6.1 - Fig. 6.2. In the case of the

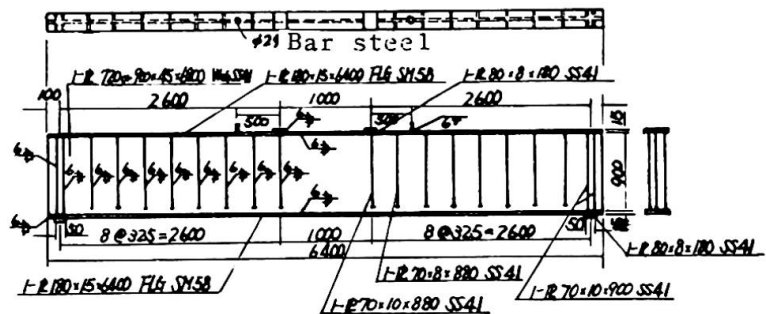


Fig. 3 Bending Test Specimen (Type G)

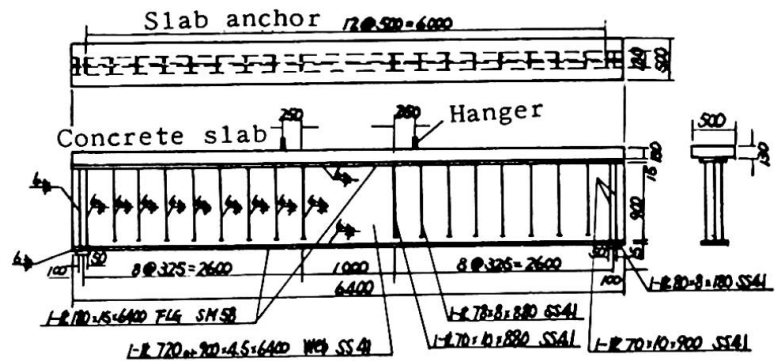


Fig. 4 Bending Test Specimen with Slab (Type GS)

Table 2. Section Performance and Value of Load

Type	Moment inertia (cm^4)	Section modulus (cm^3)	Standardized values of loads				Measured values of loads		
			Web yielding load (W_y) (ton)	Flange allowable load (F_a) (ton)	Flange yielding load (F_y) (ton)	Perfect plastic moment load (M_p) (ton)	Web yielding load	Flange yielding load	Perfect plastic moment load
G1 GS1	86.937	2318.32	42.72	46.37	78.21	80.53	62.4	110.2	113.4
G2 GS2	140.373	3018.77	55.19	60.38	100.69	103.53	81.2	142.0	146.2

test specimens made of steel alone, experimental values retains linear relations until the load (F_a in the Fig. 6) comes up to the allowable stress of the flange. Thereafter, the linear relations come to be broken gradually. This suggests that yielding of the web occurs earlier than expected at a point lower than the yielding load of the web due to the effects of the residual stress, etc. Then, deformation becomes serious rapidly and collapse occurs (shown in Fig. 6.1). Collapse was

Table 3. Results of Tension Test on Material:

Grades of steel	Thickness (mm)	Allowable stress intensity in the highway bridge specifications (kg/mm^2)	Yield strength (kg/mm^2)	Tensile strength (kg/mm^2)	Elongation (%)
SM 58	8	26.00	61.4	67.6	13.1
	6	26.00	63.1	68.6	13.9
SS 41	8	14.00	26.8	44.7	29.6
	6	14.00	29.2	43.8	26.5
	4.5	14.00	27.9	46.7	25.3

supposed to be a result of transverse buckling in type G1 and vertical buckling on the web near the loading point in type G2. In the case of type GS1 (non-composite girder) with the slab, composition of the slab and the steel girder came to be broken gradually beginning near the supports and corrugations appeared in the tension field, indicating shear buckling in the web between the loading point and the support. The concrete near the loading point collapsed when load went beyond the perfect plastic moment. Then, the steel girder beneath that part turned to be a plastic hinge and the whole body collapsed (photo 1). Type GS2 showed the same behaviors as those of type GS1 until the occurrence of shear buckling in the web. Thereafter, cracks occurred running parallel to the girder on the slab concrete and the concrete on one side came off. Under a load a little lower than the perfect plastic moment, transverse buckling occurred on the whole body of the girder.

Above behaviors can be summarized as follows:

- i) Either of type G1 or G2 girder shows elastic behavior until the load reaches the allowable stress intensity of flanges.
- ii) In the case of test specimens, types GS1 and GS2, in which transverse buckling is prevented by the attached slab, the slab concrete works well to prevent the local buckling and transverse buckling in flanges, suggesting that the hybrid girder has a bending strength up to the load for the perfect plastic moment.
- iii) From the above 2-point views, it is considered that hybrid girders may well be designed on the basis of the yield stress intensity of flanges.

4. Buckling

Among three patterns of buckling, (1) transverse buckling, (2) local buckling in compression flanges and (3) web buckling, local buckling in compression flanges was studied.

The web of a homogeneous girder, which is within the elastic region, works as a supporting member against the local buckling in a compression flanges, but in the case of hybrid girder whether or not the web works as a supporting member was left unknown. Thereupon, compression test was conducted using a cross column

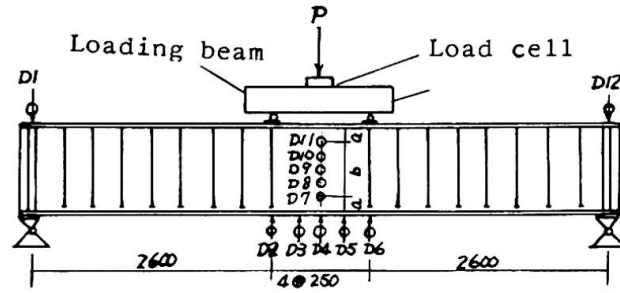


Fig. 5 Loading method for Bending Test

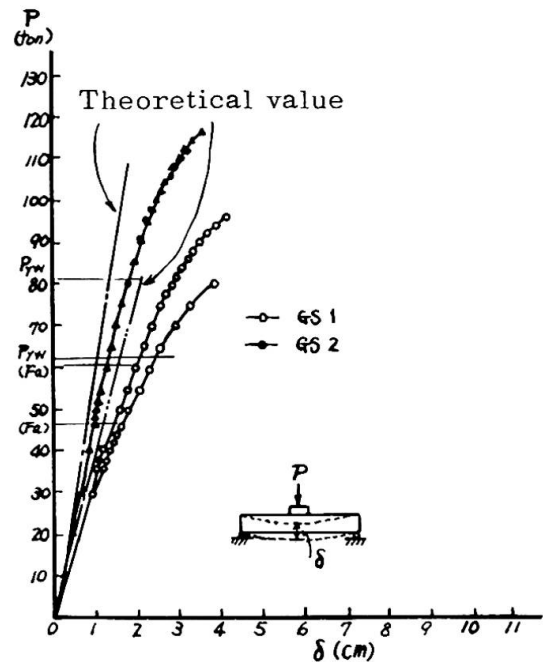


Fig. 6.1

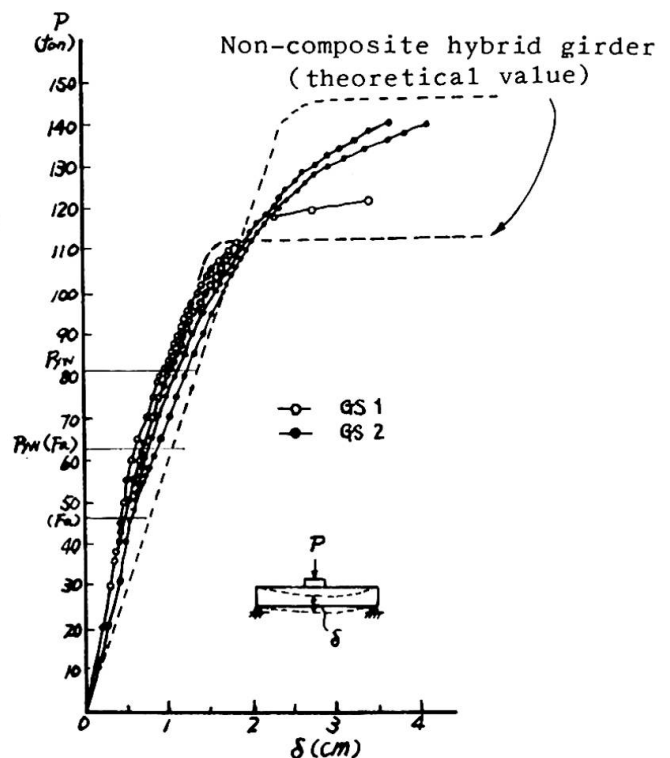


Fig. 6.2

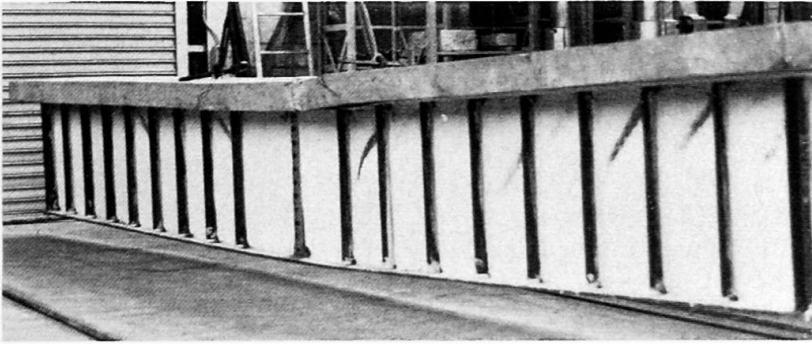


Photo. 1

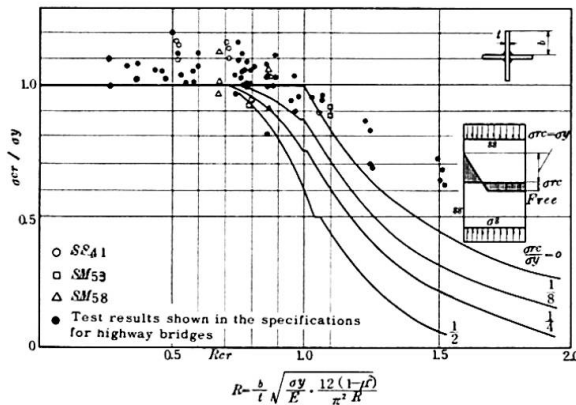


Fig. 8 Buckling Curve for Compression Hybrid Column

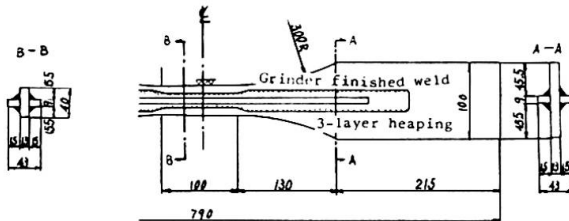


Fig. 9 Tension and Fatigue Test Piece of Hybrid Material

in a condition of high stress. Accordingly, fatigue test was made on the tension test piece of the hybrid girder made of SS41 combined with HT80 as shown in Fig.9.

A HT80 plate, 13mm in thickness, was assumed to be a flange and a SS41 rib to be a web. In order to avoid lopsided loading, ribs were fitted on both sides of the plate, and the test piece was made applying manual flat welding after pre-heating of the part at 100°C or over.

The welding rod used was low-hydrogen electrodes in use for 60 kg/mm² strength high tension steel. Perfect pulsating tension fatigue tests were made paying special attention to the fillet weld parts of HT80 flange and SS41 web. The test results are shown in Fig. 10.

The relation between the total amplitude of the stress

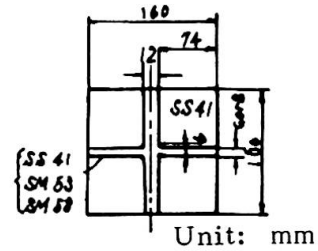


Fig. 7 Hybrid Column
Compression Test Piece

made of 3 grades of steel, SS41, SM53 and SM58 combined. The shape and dimensions of the testpieces are shown in Fig. 7.

The results of compression test on the homogeneous cross columns collected for the specifications of the highway bridges and the results of compression test on the hybrid cross columns thus made are shown in Fig. 8.

From Fig. 8 it may well be considered that the local buckling strength of a free-projecting part of the hybrid girder is the same exactly with that of the homogeneous girders.

5. Fatigue

An important problem in comparing a hybrid girder with homogeneous girder was concerned with the fillet weld (longitudinal fillet weld) to connect the web to the flange in the neighborhood of which the web is

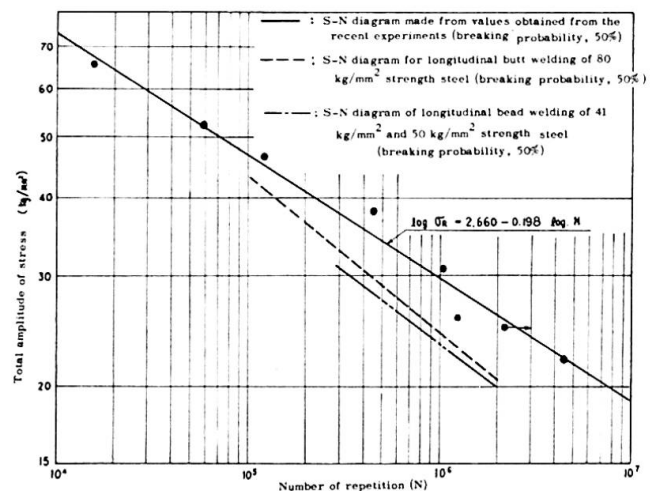


Fig.10 S-N Diagram of Hybrid Material

σ_R (kg/mm², in calculation of the stress, the section of the base metal was considered in disregard of that of the weld metal) and its number of repetition (N) was obtained as follows by the method of least square

$$\log \sigma_R = 2.660 - 0.198 \log N$$

The value of fatigue strength is a little higher than that in the data on fatigue strength obtained in the past in the longitudinal fillet weld applied to mild steel of 40 kg or 50 kg/mm² strength steel and 80 kg/mm² strength steel.

From the foregoing, the fillet weld fatigue strength of flanges and webs of hybrid girders can be regarded same as that of homogeneous girders.

6. Conclusion

- 1) According to the combination of several grades of steel, hybrid girders become economical occasionally more than 10 percent as compared with homogeneous girders.
- 2) Hybrid girders can be designed on the basis of the yield stress intensity of flanges.
- 3) As the local buckling on the compression flange is considered same as in the case of homogeneous girders, the existing provisions can be applicable to the thickness of outstanding parts of the compression flanges.
- 4) The fatigue strength of the fillet weld portion connecting the web to the flange can be regarded same as that of homogeneous girders.

Postscript

Mentioned above are the results of our experiments on the bending characteristics, buckling and fatigue that occurred in hybrid girders.

Under judgement that from the foregoing it is possible to make out the design standards for the hybrid highway bridges based on the provisions of the existing specifications for highway bridges, we have been proceeding with the work therefor. At the same time we will continue studies on the aforementioned problematical points left unsolved.

Furthermore, we plan to compare from economical viewpoint the bridges made under said standards with those built under the existing standards, and then enter into further details of the economical efficiency of the hybrid girders.

SUMMARY

Economic efficiency and design problems of hybrid girders are studied. It is economical when mild steel and strength steel exceeding 58 kg/mm² are combined. Bending behaviour, buckling strength of compression flanges and fatigue strength of fillet welds between flanges and webs for hybrid girders are studied. As a result, hybrid girders can be designed by extending the present design methods on homogeneous girders.

RESUME

Une étude a été faite au sujet des problèmes d'économie et de conception des poutres hybrides. Lorsque l'acier doux et l'acier ayant une résistance de plus de 58 kg/mm² sont associés, une économie peut être réalisée. Le comportement à la flexion, la résistance au flambage des ailes comprimées et la résistance à la fatigue des soudures entre les ailes et les âmes ont été étudiées pour les poutres hybrides. Le résultat montre qu'il est possible de calculer des poutres hybrides en appliquant la conception actuelle pour les poutres homogènes.

ZUSAMMENFASSUNG

Wirtschaftlichkeit und Entwurfsprobleme von hybriden Tragbalken werden untersucht. Wenn Baustahl St 37 und Stahl mit einer Festigkeit über 58 kp/mm² kombiniert werden, ist dies wirtschaftlich. Das Biegeverhalten, die Kippsicherheit und die Dauerfestigkeit der Kehlnähte zwischen den Flanschen und Stegen der hybriden Tragbalken werden untersucht. Daraus folgt, dass hybride Tragbalken durch Erweiterung der vorliegenden Entwurfsmethoden auf homogene Tragbalken angewendet werden können.

Structural Behaviour of Hybrid Plate Girders in Bending. Application to Actual Bridges

Comportement à la flexion de poutres à âme pleine hybrides.
Application aux ponts actuels

Biegeverhalten von hybriden Vollwandträgern.
Anwendung im Brückenbau

Y. MAEDA
Professor of Civil Engineering
Osaka University
Suita, Osaka, Japan

M. ISHIWATA
Senior Engineer
Kawasaki Steel Co., Ltd.
Tokyo, Japan

Y. KAWAI
Research Engineer
Kawasaki Steel Co., Ltd.
Chiba, Japan

I Introduction

At the IABSE London Colloquium in 1971, the ultimate strength of hybrid girders was discussed, and especially the fatigue study on thin-walled hybrid girders was encouraged.

The present study is intended to discuss the static and fatigue behavior of thin-walled, stiffened hybrid girders based on the results of tests carried out at Osaka University. Furthermore, to apply the hybrid girder to long-span bridges, its design and economy are discussed with actual and design illustrations.

II Structural Behavior and Strength

II-1 Static Behavior and Strength

The overall flexural behavior of thin-walled hybrid girders consisting of WES-HW70, JIS-SM58 and JIS-SS41 in tension flange, compression flange and web, respectively, (1) is summarized in Fig. 1 in terms of the relation between applied bending moments and measured curvatures, to study on the influence of web slenderness ratios on the static flexural behavior. In Fig. 1, the calculated moment-curvature curves taking into account measured residual stresses and those neglecting the residual stresses are also given to show the effect of residual stresses. It can be seen in Fig. 1 that the girders with web slenderness ratios less than about 200 will behave like stocky beams owing to single horizontal stiffener located at one-fifth of the web depth, and that the test curves agree fairly well with the calculation curves with residual stresses. In the case of more slender girders of which web slenderness ratio exceeds about 250, however, the additional decrease of rigidity caused by web buckling diverts the test curves from the calculation curves.

Table 1. Ultimate strength and reference loads

Girder	α	β	M_u/M_u^*	M_u/M_{yw}^{th}	M_u/M_{yf}^{th}	M_u/M_p^{th}
AL 1	0.5	141	1.18	3.42	1.18	1.16
BL 1	1.0		1.23	3.29	1.23	1.11
AL 2	0.5	188	1.10	3.09	1.10	1.08
BL 2	1.0		1.09	3.09	1.09	1.06
AL 3	0.5	232	1.15	3.14	1.15	1.12
BL 3	1.0		1.07	2.97	1.07	1.05
AL 4	0.5	281	1.05	2.72	1.01	0.99
BL 4	1.0		1.04	2.70	0.99	0.97

α : Aspect ratio of test panel, β : Web slenderness ratio

M_u^* : Experimental ultimate moment, M_u^* : Predicted ultimate moment

M_{yw}^{th} : Theoretical web yield moment,

M_{yf}^{th} : Theoretical flange yield moment

M_p^{th} : Theoretical fully plastic moment

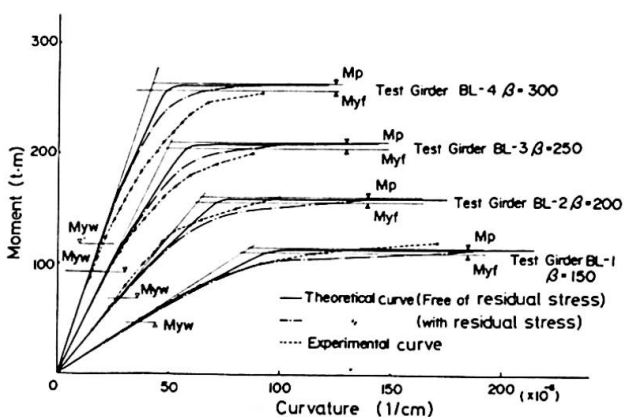


Fig. 1. Moment v.s. curvature curve

The experimental ultimate loads and the several reference loads calculated by the ordinary beam theory are shown in Table 1, which indicates that the limiting web slenderness ratio β with which a girder carries its theoretical flange yield moment is 323 and 289 for the aspect ratio α of 0.5 and 1.0 respectively. In Table 1, there are also the ultimate bending moment M_U^* predicted by a formula (1) which can estimate the decrease of resisting moment due to web buckling, and such prediction seems to be conservative.

According to the AASHTO Specifications (3), an allowable stress in a tension flange should be reduced depending upon the spreading of web yielding so that the slight decrease of rigidity of a girder due to web yielding can be estimated in design. Since such reduction, however, is derived from stress distribution on a cross section when its tension flange yields, yielded region in the web can be controlled relatively small to a primarily assumed extent in design. In Table 2, comparisons among the experimental ultimate moment (1), the design allowable moment and also the design ultimate moment to be examined at the assumed ultimate state in Load Factor Design (3) are shown. It is revealed that the experimental ultimate moment agrees well with the design ultimate moment and amounts to more than twice as much as the design allowable moment.

II-2 Fatigue Behavior and Strength

Concerning static behavior and strength, it proved that a thin-walled hybrid girder with a web slenderness ratio less than about 290 could be dealt with as a homogeneous girder, only considering the slight decrease of rigidity due to web yielding. On structural behavior under repeated bending, however, the fatigue peculiar to a thin-walled plate girder that is caused by out-of-plane movement of a slender web, has been studied by Yen, Stallmeyer, Toprac and Maeda, etc.

Fig. 2 shows typical patterns of fatigue crack initiated in a hybrid girders subjected to pure bending. Among these types of crack, Type 1 cracks are the cracks above mentioned and were actually observed in the extensive fatigue tests of hybrid girders made by Toprac (8), who suggested that it is effective to use horizontal stiffeners and/or to limit the web slenderness ratio to be less than 200 for prevention of the initiation of Type 1 cracks.

In Table 3, the results of fatigue tests of six large-sized hybrid girders conducted by authors (13) are summarized together with parameters to evaluated the test results. All of the test girders failed due to Type 2 cracks initiated at the toe of vertical stiffener-to-web fillet welds. Type 1 crack and Type 3 crack were also observed in Girders B4-L1 and B3-L1, they were not a governing crack to cause the failure of the girders.

The regression analysis based on the method of least squares for the test results obtained by authors (10) and Toprac (8) with regard to the initiation of Type 2 cracks, gives the fatigue strength

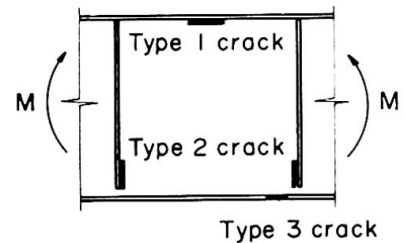


Fig. 2. Types of fatigue cracks under pure bending

Table 2. Comparisons of ultimate moment with design moment

Girder	M_U^{ex}	AASHTO				M_{yw}	M_U^{ex}/M_{all}	M_U^{ex}/M_U
		R	Fail	M_{all}	M_U			
AL 1	130	0.85	30.9	47.7	104	38	2.73	1.25
BL 1	125						2.62	1.20
AL 2	170	0.83	29.9	66.9	146	55	2.54	1.16
BL 2	170						2.54	1.16
AL 3	232	0.81	29.0	87.1	191	74	2.66	1.22
BL 3	220						2.52	1.15
AL 4	258	0.79	28.4	109.5	240	95	2.36	1.08
BL 4	257						2.35	1.07

M_U^{ex} : Experimental ultimate moment (t·m)

M_{all} : Allowable bending moment (service load design) (t·m)

M_U : Design ultimate moment (load factor design) (t·m)

R: Reduction factor

M_{yw} : Experimental web yield moment (t·m)

F_{all} : Allowable stress in tension flange (kg/mm^2)

Table 3. Test parameters and test results

Test Girder	β	t/I^*	S_r	R	Type of crack, N_c			Mode of failure
					Type 1	Type 2	Type 3	
B4L1	413	1	21.1	0.221	465	34.1	—	Type 2
B4L7		7	23.1	0.209	—	243	—	Type 2
B3L1	310	1	a) 11.7	0.543	—	218.0	218.0	Type 2
B3L6		6	21.1	0.402	—	28.0	—	Type 2
B2L0	206	—	17.6	0.439	—	104.0	—	Type 2
B2L5		5	16.1	0.456	—	116.6	—	Type 2

β : Web slenderness ratio

t/I^* : Relative rigidity ratio of horizontal stiffener

S_r : Stress range in tension flange (kg/mm^2)

R: Stress ratio, N_c : Number of cycles to crack ($\times 10^4$)

a) Maximum stress was increased up to 35.1 kg/mm^2 after 2,100 cycles

at 2×10^6 cycles in terms of stress range with 12.9 kg/mm^2 (mean value) and 10.7 kg/mm^2 (95% confidence limit) which is more than 25% above the allowable stress range of 8.4 kg/mm^2 (Stress Category: C) at the AASHTO Specifications. It is recognized that the fatigue strengths due to Type 2 crack and Type 3 crack can be respectively compared to those of a transverse non-load carrying fillet welded joint and a longitudinal fillet welded joint (4,7). Since the fatigue strength at 2×10^6 cycles of the latter joint is 30 to 50% higher than that of the former joint. According to a great number of fatigue tests (11), it may be concluded that Type 1 crack and Type 2 crack characterized the fatigue behavior of thin-walled hybrid girders with vertical stiffeners. As shown in Fig. 3, the test results of transverse non-load carrying fillet welded joints for several steel grades (12) agree well with those of Type 2 cracks at the girder tests (10), and the both fatigue strengths do not significantly differ from each other depending on the steel grades, covering 9 to 13 kg/mm^2 . Consequently, it proves that a web in ordinary carbon steel is the most economical for a thin-walled hybrid girders as far as the fatigue strength is limited to the fatigue life of Type 2 crack.

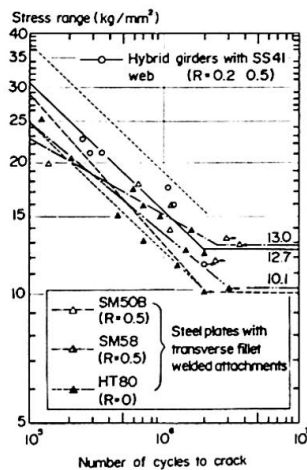


Fig. 3. S-N curves for Type 2 crack

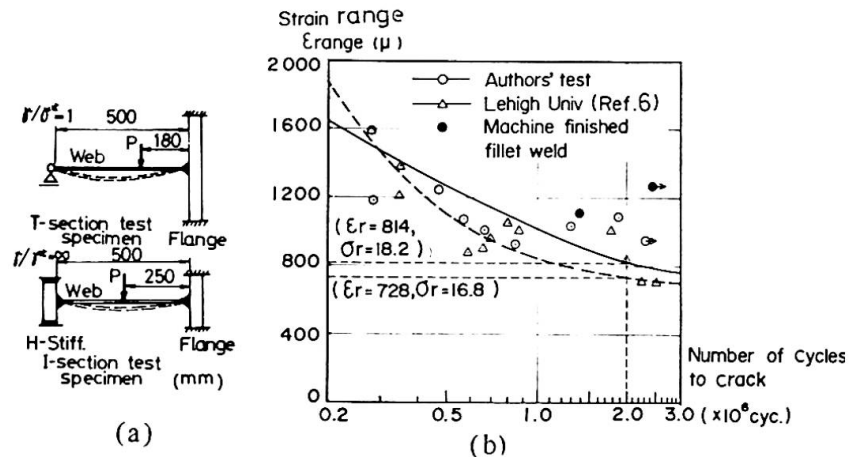


Fig. 4. Fatigue test results for Type 1 crack

On the other hand, few comparable tests for Type 1 crack have been carried out on model specimens of Type 1 crack, because of complicated cracking conditions. In Fig. 4, the relevant results obtained at fatigue tests made by Maeda (14) on model specimens of a web panel enclosed by a compression flange and a horizontal stiffener as shown in Fig. 4(a), are shown in terms of the number of cycles to crack initiation and the local strain range at the toe of fillet weld estimated by F.E.M. plate analysis combined with strain measurements. Available data of fatigue tests of large-sized plate girders conducted by Ostapenko (13) are also given, but they seem considerably dispersed, attributed to inevitable inherent indentations at the toe of fillet weld.

The fatigue strength at 2×10^6 cycles of the fillet weld under bending is estimated to be 814×10^{-6} in strain range or 18.2 kg/mm^2 in stress range with the regression analysis by the method of least squares. To examine the relation between the magnitude of out-of-plane deflection of a web and the fatigue lives of Type 1 crack, a non-dimensional parameter δ_r/h which represents the ratio of web deflection range to panel depth, is introduced. With this parameter the fatigue strength of Type 1 crack is rearranged graphically as shown in Fig. 5. The figure suggests that the magnitude of out-of-plane deflection of a web under a repeated live load should be limited to $1/350$ of a web panel depth. To find out the governing

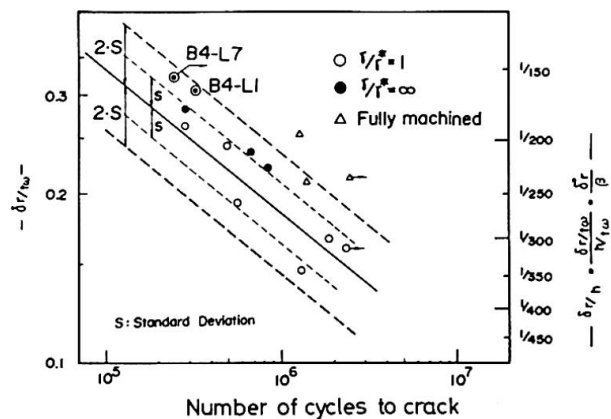


Fig. 5. Relation between magnitude of out-of-plane deflection of a web and fatigue lives of Type 1 crack

design criterion of Type 1 crack, it is desirable to develop the relevant fatigue data to induce the relation between the maximum initial web deflections, δ_0 , and the out-of-plane movements, δ_r , under applied live loads in terms of $\delta_r/h = f(\sigma, \delta_0, \gamma/\gamma^*)$, where σ is the calculated bending stress at the extrem fiber of the web and γ/γ^* is the ratio of the relative rigidity ratio of the horizontal stiffener.

III Application of Hybrid Girders to Highway Bridges

Two composite hybrid girder bridges constructed in Japan are introduced in Table 4 as examples of actual highway bridges. Furthermore, including these bridges, the strength and economy of composite and non-composite hybrid girder bridges are discussed.

III-1 Design Problems

In design of hybrid girders, a reduction factor, R , specified at the AASHTO Specifications (3), was used to take into consideration the slight decrease of flexural rigidity due to web yielding; to prevent overstressing at erection, calculated dead load bending stresses at the extreme fiber of web, were limited to 80% of its specified yield stress; and web slenderness ratio were modified with a coefficient \sqrt{R} . It is found out that the reduction factor, R , is the most fundamental governing parameter to estimate a flange allowable stress, a web slenderness ratio and even economy of the hybrid girder, and that a further study on the reduction factor R is required.

Regarding fatigue design, it is proved that the initiation of Type 1 crack can be prevented as far as the web slenderness ratio discussed at the previous chapter, are used (1, 10), and Type 2 crack can be prevented if a calculated bending stress at the end of vertical stiffener does not exceed at an allowable fatigue stress at transverse non-load carrying fillet welds. In addition to these cracks, Type 3 crack will be kept away by well controlled welding operations.

III-2 Economy

In Japan, a number of structural steels in various grades can be put to practical use, and a choice of grade of steel, from JIS-SS41 to WES-HW80, is within a designer's choice.

Economy of hybrid girders was examined for hybrid composite girders and non-composite continuous girders in terms of overall costs for combination of different steel grades. The overall costs of the girders including material, fabrication and erection costs were calculated with the costs recommended at the Japan Bridge Construction Association (1972).

Table 4. Composite hybrid girder bridge in Japan

		ARAI Bridge	SORO Bridge
Span (m)		19.2	33.0
Steel sets	U.Flange	Center SM50	Center SM50Y
	Web	SS41	SS41
	L.Flange	HW70	SM58
Reduction factor		$R = 0.721$ (SS41 - HW70)	$R = 0.877$ (SS41 - SM58)
Completed time		June 1974	April 1976

Table 5. Design requirements

Loading	TL-20
Road width (m)	$7.5 + 2 \times 1.5$ (footway)
Span (m)	26, 32, 36, 44
Web depth	$0.9h_w, 1.0h_w, 1.1h_w$
Steel sets	A, B, C, D, (Table 6)

h_w : Web depth of standard design

(1) Hybrid composite girders

Economical comparisons of hybrid composite girders with homogeneous ones were conducted under such design conditions as shown in Table 5. Structural proportions of homogeneous composite girders were designed based on the "Standard Design of Composite Girder Bridges (1972)", published at the Ministry of Construction in Japan.

The relationship between bridge spans and steel weights per unit area in various sets of steel with a girder depth of $1.0 h_w$, are indicated in Fig. 6. A study of Fig. 6 reveals that the weight for all of the steel sets of the hybrid girders except 'A' are lighter than those of the homogeneous girders by the

standard design. Especially, the weight of the 'D' set is the lightest among the steel sets for spans longer than 38 meters.

A comparison of overall costs of the hybrid girders with those of the homogeneous girders for various steel combination in Table 6, is shown in Fig. 7 with regard to bridge spans.

It can be said that the economy of hybrid girders is noticeable for the steel combination of 'D', 'C', 'B' and 'A' in this order, and 'D' of which cost ratio (=hybrid/homogeneous) is 0.93, will be the most economical.

Table 6. Steel sets for comparative design

	Standard design	A	B	C	D
Upper flange	SM50Y	SM50	SM50	SM50	SM58
Web	SM50Y	SS41	SS41	SM41	SM41
Lower flange	SM50Y	SM50	SM58	HW70	HW70
Web height	h_w	$0.9h_w, h_w, 1.1h_w$			h_w

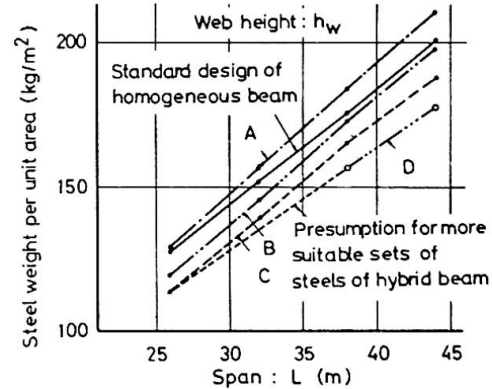


Fig. 6. Weight comparison of hybrid composite girders with homogeneous ones

(2) Three-span continuous non-composite girders

A cost comparison was carried out on three-span continuous non-composite girders with two kinds of equal span, namely 60 meters and 70 meters, under the same design requirements as the former examples. Girder depth in this comparison are fixed to one-twenty first of each span. Consequently, it is proved that hybrid girders can save 3% to 7% in overall cost more than homogeneous girders as shown in Table 7.

Table 7. Cost ratio (Hybrid/Homogeneous) for steel sets

		Homogeneous	Hybrid I	Hybrid II ^{a)}
Steel set	U. Flange	SM50Y	SM58	HW70(SM58)
	Web	SM50Y	SM41	SM41(SS41)
3 x 60 m	L. Flange	SM50Y	SM58	HW70(SM58)
	Total weight (t)	495	465	428
180 m	Cost ratio	1.00	0.94	0.97
3 x 70 m	Total weight (t)	671	627	586
	Cost ratio	1.00	0.93	0.97

a) () is for section at center span

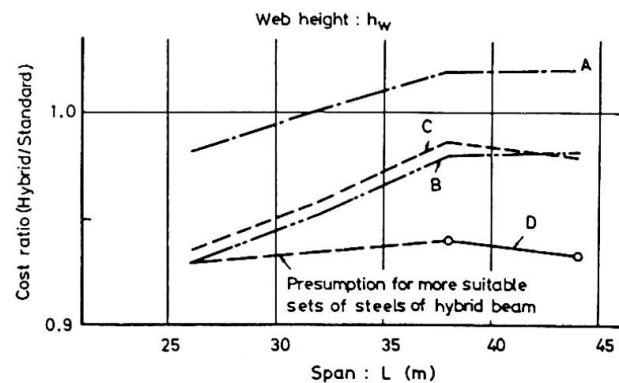


Fig. 7. Cost comparison of hybrid composite girders with homogeneous ones

IV Conclusion

It is concluded for the static behavior that the ultimate flexural strength of hybrid girders can be evaluated well by the reduction factor formula specified at the AASHTO Specifications and their flange yield moment can be carried with single horizontal stiffener up to their web slenderness ratio of about 320 and 290 for the aspect ratio of 0.5 and 1.0, respectively.

There is a possibility of initiation of Type 1 or Type 2 fatigue crack, but the former crack can be prevented for 2×10^6 cycles of loading by limiting out-of-plane movement of web, and the latter

crack by controlling a tensile web stress below the fatigue strength of transverse non-load carrying fillet welded joints.

It has been found out that hybrid girder bridges are generally more economic than homogeneous girder bridges in terms of overall cost, particularly at composite girder bridges, but in long-span continuous plate girders it is required to do more detailed comparison between hybrid and homogeneous girder bridges.

References

- 1) Y. Maeda and Y. Kawai, 18th Conf. of Bridge and Structural Eng. in Japan, 1971, p137
- 2) F. Nishino *et al.*, JSSC, Vol. 7, No. 71, 1971, p1-10, (*in Japanese*)
- 3) Standard Specifications for Highway Bridges, AASHTO, 11th Edit., 1973
- 4) W. H. Munse and J. E. Stallmeyer, Br. Weld J., 5, 188, 1960
- 5) T. R. Gurney and C. C. Woodley, Br. Weld J., Vol. 7, 1960 and Vol. 9, 1962
- 6) B. T. Yen, Fritz Eng. Lab. Rpt., No. 303.1, Lehigh Univ., Nov., 1963
- 7) L. R. Tall and J. E. Stallmeyer, Univ. of Illinois, C. E. Studies SRS, No. 279, 1964
- 8) A. A. Toprac and M. Natarajan, Proc. of ASCE, Vol. 97, ST4, 1971
- 9) Y. Maeda, IABSE Colloquium, London, 1971
- 10) Y. Maeda, M. Ishiwata and Y. Kawai, IIW. Doc. XIII-734-74, April, 1974
- 11) T. R. Gurney and S. J. Maddox, The Welding Institute Research Rpt., E/44/72, 1972
- 12) JSSC, Vol. No. 72, 1971 (*in Japanese*)
- 13) S. Parsanejad and A. Ostapenko, Lehigh Univ., Fritz Eng. Lab. Rpt. No. 156, Nov., 1970
- 14) Y. Maeda *et al.*, Preprints Papers 30th Annual Conf. of JSCE, 1975 (*in Japanese*)

SUMMARY

For the purpose of optimum use of high-strength steels, static and fatigue behaviour of thin-walled, stiffened plate girders are studied. Design and economy of hybrid girders bridges are discussed with illustrations.

RESUME

Le comportement statique et de fatigue des poutres à âme pleine, mince et raidie est étudié en vue de l'utilisation optimum des aciers à haute résistance. Le calcul et l'économie de ponts à poutres hybrides sont discutés et illustrés.

ZUSAMMENFASSUNG

Zur optimalen Verwendung der Hochfestigkeitsstähle werden das statische Verhalten sowie Ermüdungsverhalten dünnwandiger und verfestigter Vollwandträger untersucht. Wirtschaftlichkeit der Vollwandträgerbrücken werden zusammen mit Bildern erörtert.

Fatigue Strength of Longitudinal Fillet Welded Joints in Hybrid Girders

Résistance à la fatigue des soudures d'angle, dans les poutres hybrides

Dauerfestigkeit der Längskehlnähte bei hybriden Vollwandträgern

T. YAMASAKI
General Manager

M. HARA
Senior Research Engineer

Y. KAWAI
Research Engineer

Steel Structure Research Laboratories, Kawasaki Steel Co., Ltd.
Chiba, Japan

I . Introduction

In this decade several investigations were conducted to study static and fatigue strength of hybrid girders in U. S. A. (1~6) and Japan (7~9), and some of these data were adopted into design specifications for U. S. highway bridges (10) and buildings (11).

On fatigue strength of hybrid girders, Toprac et al. pointed out based on their significant experimental study that there are three distinctive types of fatigue cracks, initiated at different locations and by different causes in hybrid girders under pure bending, as shown in Fig. 1. (5). Regarding Type 3 crack, Specifications for Highway Bridges in U. S. A. (10) specifies that stiffener to web and flange-web fillet weld connection shall be designed for fatigue based on the flange steel.

The purpose of the present work is to explore the data of fatigue strength of Type 3 crack in hybrid girders and to study the crack propagation behavior at tension flanges and webs. Test results obtained by model specimens are discussed on fatigue strength with reference to structural behavior of hybrid plate girders subjected to repeated bending by usual analytical procedures (S-N relations) and fracture mechanics.

II. Test Specimens and Procedures

Test specimens and test procedures were simulated to those proposed by Reemsnyder (13) by using tee-shaped hybrid specimens consisting of WES-HW 70 (heat treated constructional alloy steel with minimum specified tensile strength of 80 kg/mm^2) at simulating flange plates and JIS-SS41 (structural carbon steel with minimum specified tensile strength of 41 kg/mm^2) at simulating web plates, under axial pulsating tension.

Ten axially loaded fillet welded tee-shaped specimens were tested at a stress ratio of $R=0.1 (\div 0)$ (one of these was a large-sized specimen), and four were at a stress ratio of $R=0.5$. These specimens were submerged-arc welded with an intermediate strength filler metal-flux combination. The lower strength filler metal-flux combination than flange steel is preferred the fillet welding between constructional alloy steel and mild steel because of its economy and its

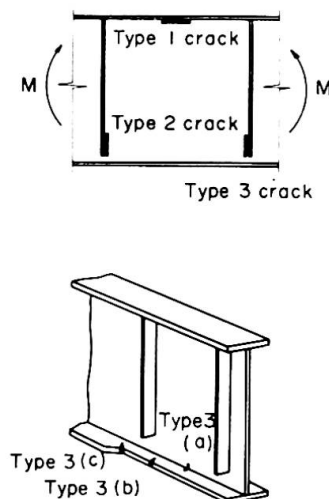


Fig. 1 Types of fatigue cracks under pure bending

ductility (7, 13). No non-destructive inspections, radiography or ultra-sonic inspection were performed before fatigue testing, assuming that the most unfavourable conditions existed. Details of the tee-specimens are shown in Fig. 2, and the mechanical properties and chemical compositions are summarized in Table 1.

All specimens were tested in 150-ton electro-hydraulic alternating testing machine at about 300 c.p.m. and applied stresses during fatigue test were monitored by dynamic strain measurements and a load cell and fatigue crack propagations were measured by using crack gauges when fatigue crack initiations were observed.

Table 1. Mechanical properties and chemical compositions

	Thickness (mm)	Chemical Compositions (Wt %)												Mechanical Properties			
		C	Si	Mn	P	S	Cu	Ni	Cr	Mo	V	B	Ceq	Y.P. kg/mm ²	U.T.S. kg/mm ²	Elong. (%)	Y.E. kg-m
WES-HW70 (Base Plate)	16	0.100	0.30	0.85	0.007	0.010	0.19	0.78	0.46	0.33	0.035	0.004	0.45	80	84	32	15.6
JIS-SS41 (Rib Plate)	12	0.14	0.033	1.17	0.009	0.021	—	—	—	—	—	—	—	29	47	35	—
Weld Metal (KW-101B)	φ 4	0.06	0.24	1.45	0.013	0.009	—	0.77	—	0.41	—	—	—	57	66	26	—

III. Test Results and Discussion

III-1 Test Results

The fatigue test results are summarized in Table 2 and are shown graphically in Fig. 3. All the test results are discussed in relation to applied stress range at welds S_r and number of cycles to failure N_f .

Although the test results at different stress ratios of $R=0$ and $R=0.5$ are plotted irrespectively, the data fall in a certain scatter band. Judging from this fact, the effect of mean stress may be neglected in these stress ratios of 0 to 0.5. The regression analysis of all the present test results obtained by the method of least squares with reference to the number of cycles to failure and the stress range gives eq. (1).

$$\text{Log } N_f = 11.790 - 4.218 \text{ Log } S_r \dots\dots\dots (1)$$

Table 2. Summary of Test Results

No	TEST PIECE	APPLIED STRESS (kg/mm ²)			STRESS RATIO (R.)	FIRST OBSERVATION (x10 ⁴)	CYCLES TO FAILURE (x10 ⁴)	CRACK INITIATION MODE ^{b)}
		MAX (S _{max})	MIN (S _{min})	RANGE (S _r)				
1	T.P.-No.1	25.9	2.7	23.2	0.1	—	124.50	N
2	T.P.-No.2	28.8	2.8	26.0		88.11	91.65	W
3	T.P.-No.3	33.8	3.2	30.6		24.85	26.17	N
4	T.P.-No.4	20.8	2.2	18.6		—	267.2 ^{d)}	—
5	T.P.-No.5	21.4	2.1	19.3		—	228.20	C
6	T.P.-No.7	32.4	3.1	29.3		—	43.00	W
7	T.P.-No.8	24.1	2.3	21.8		205.62	212.60	W
8	T.P.-No.9	34.3	1.6	32.7		26.23	27.04	W
9	T.P.-No.12	23.2	2.3	20.9	0.5	91.00	93.92	W
10	T.P.-No.6	47.4	24.2	23.2		154.13	158.02	W
11	T.P.-No.10	40.4	19.7	20.7		162.50	166.88	C
12	T.P.-No.11	52.2	26.6	25.6		—	41.91	C
13	T.P.-No.13	36.7	18.0	18.7		—	263.52 ^{d)}	—
14	T.P.-No.14	19.5	1.7	17.8		0.1	257.00 ^{d)}	—

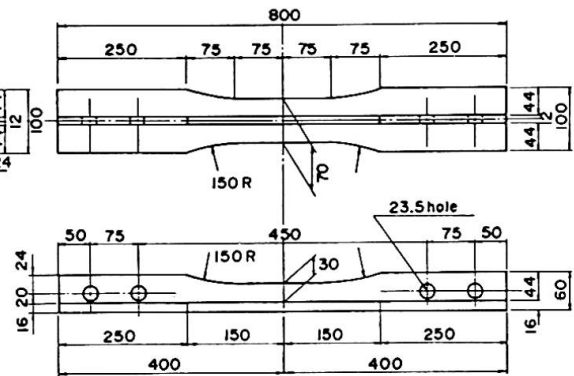
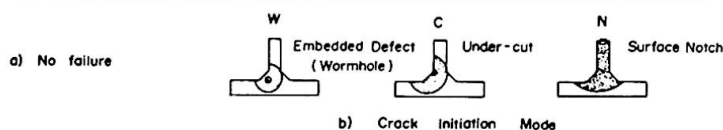


Fig. 2 Details of test specimen

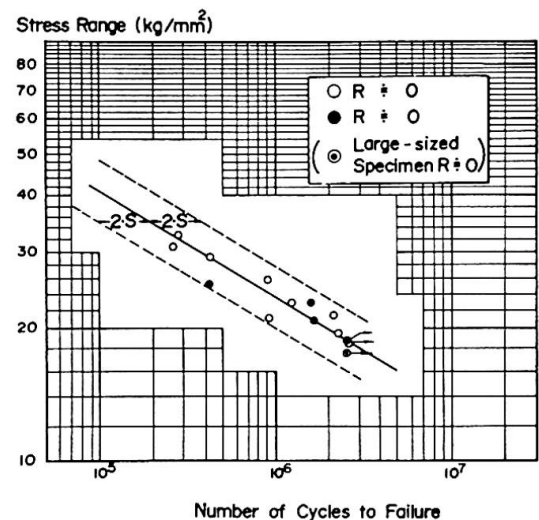


Fig. 3 Fatigue test results

The mean regression line is shown in Fig.3 together with its confidence limits. The fatigue strength at 2×10^6 cycles in stress range are estimated at 20.0 kg/mm^2 (mean) and 16.9 kg/mm^2 (95% confidence limit). The behavior of cyclic specimens was very consistent in spite of the fact that yielding was occurred at web plates in the several specimens subjected to higher maximum stresses.

The observed crack initiation modes were divided into three types and the mode applying to any specimen is recorded in Table 2 and typical fracture surface of three types of crack initiations are shown in Figs. 4 to 6. Among these initiation modes, the most frequent initiation was type W, and this fact agreed with the fatigue test results of homogeneous beams by Fisher et al. (14).

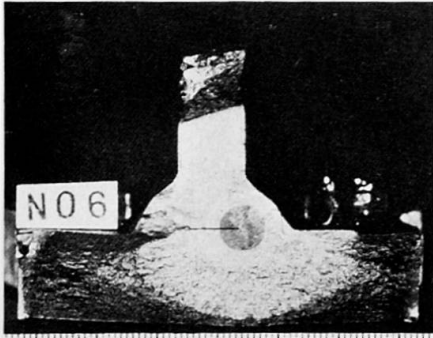


Fig. 4 Fracture surface
(from worm-hole)



Fig. 5 Fracture surface
(from under-cut)

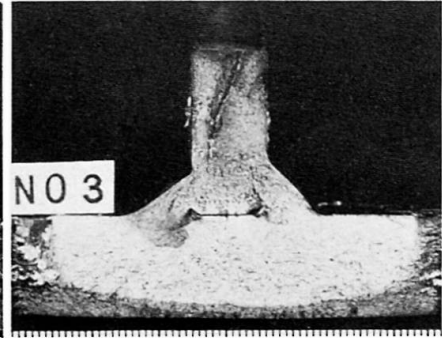


Fig. 6 Fracture surface
(from surface notch)

III-2 Comparisons with Previous Fatigue Data

The fatigue data of hybrid girders can be conventionally compared with those of homogeneous ones (5,6). There are several investigations into the fatigue strength of high strength steel girders and longitudinal fillet welded joints comparable with the present test results. The comparisons between these fatigue strength were extensively discussed in Ref.(15). Fig.7 shows the additional comparisons with these available fatigue data for analysis of Type 3 crack. In particular, the work by Reemsnyder (13) on the fatigue strength of longitudinal fillet weld in constructional alloy steel is most comparable, because the present test pieces and test procedure are simulated to those of that work. The two test

results shown in Fig.7, that is, solid circles and the hollow circles represent the test results obtained by using hybrid specimens and homogeneous ones respectively, and they seem to agree well with each other in spite of disregarding the effect of the mean stress. Again, a study of Fig.7 reveals that the fatigue strength of tee-shaped model specimens and those of beams consisting of 80 kg/mm^2 class high strength steel are not significantly different.

Furthermore, there are two other comparable previous works that are essential. Fig.8(a) and Fig.8(b) are quoted from these works by Frost(4) and Toprac(5), respectively. Both figures represent the comparisons between the test results

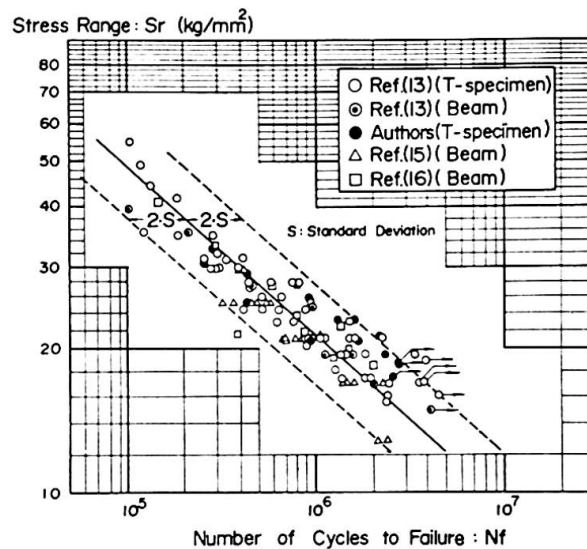


Fig. 7 Comparison of previous work on Type 3 crack
with this study

of hybrid girders consisting of 80 kg/mm² class high strength steel in flanges (4,5) and these of tee-shaped homogeneous specimens (13). It seems that the former ones are slight higher than the latter, especially in the case of Fig. 8(b). The disagreement in Fig. 8(b) was concluded by Toprac that such a difference could be attributed to the fact that the tee-shaped specimens were fabricated under a controlled condition, whereas the girder specimens were fabricated with an average commercial shop practice. This conclusion implies that the fatigue strength, especially regarding to Type 3 crack, is largely influenced by welding conditions and fabrication methods.

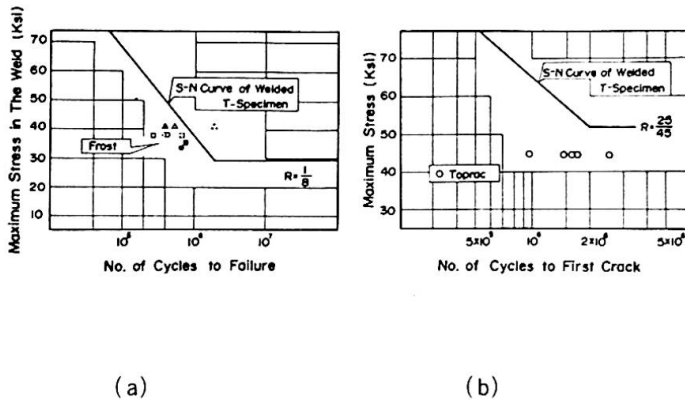


Fig. 8 Comparison of fatigue data on hybrid beams with homogeneous tee-shaped specimens

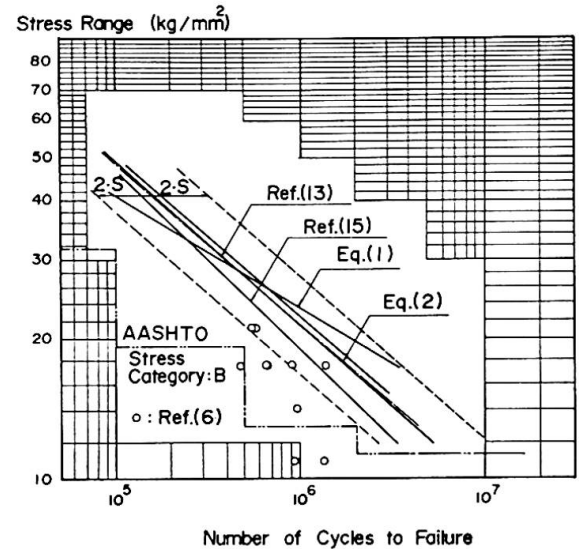


Fig. 9 Comparison of related S-N curves with design stress

The regression analysis of all the available test results by the method of least squares gives

$$\log N_f = 9.720 - 2.800 \log S_r \quad \dots \dots \dots (2)$$

and fatigue strengths at 2×10^6 cycles of web-to-flange fillet welded joints consisting of 80 kg/mm² class high strength steel in flanges are estimated at 16.7 kg/mm² (mean) and 12.9 kg/mm² (95% confidence limit) in stress range. Shown in Fig. 9 is all the available S-N curves related to longitudinal fillet weldments in web-to-flange junctures, using the mean regression lines and the limits of dispersion corresponding to the 95% confidence limits in comparison with fatigue allowable stresses specified in AASHTO Specifications.

It will be reasonable, if Toprac's result is ignored, that the clause in AASHTO (10,17) provides that web to flange weld connections in hybrid girders shall be designed for preventing fatigue based on the flange steel and that allowable fatigue stresses are given in terms of stress ranges.

III – 3 Fatigue Behavior Prediction by Fracture Mechanics

The relation between the fatigue crack-growth rate and the change in the stress intensity factor is presented in the form of

$$da/dN = C(\Delta K)^m \quad (\text{mm/cycle}) \quad \dots \dots \dots (3)$$

where a is a half length of fatigue crack and ΔK the variation of the stress intensity factor ($K_{max} - K_{min}$); C and m are material constants. And, the stress intensity factor usually takes the form

$$K = \sigma \sqrt{\pi a} \cdot f(a) \quad (\text{kg/mm}^{-3/2}) \quad \dots \dots \dots (4)$$

where σ and $f(a)$ respectively represent remotely applied stress and a correction function to which the dimensions of the plate, the distance to a free edge or surface and the shape of cracks are introduced. From eqs. (3) and (4), the fatigue life N is given as

$$N = \frac{1}{C(\Delta \sigma)^m} \int_{a_i}^{a_f} \frac{da}{a^{m/2} \cdot \pi^{m/2} \cdot f^m(a)} \quad \dots \dots \dots (5)$$

where a_i and a_f are the initial and final crack sizes, respectively. On the other hand, the conventional S-N relation is represented as follows

$$\text{Log } N = C' - n \cdot \text{Log}(\Delta\sigma) \quad \dots\dots\dots (6)$$

where N and $\Delta\sigma$ are the fatigue lives and the applied stress ranges respectively and C' and n are material constants. Fisher et al. (14) introduced the relationship among these constants, in eqs. (3) and (6) that characterize the fatigue crack growth rate and the S-N curve, respectively, as follows.

$$m = n \quad (7-a)$$

and

$$C' = \text{Log} \left[\frac{1}{C} \cdot \frac{(a_i^{-\alpha} - a_f^{-\alpha})}{\alpha \cdot f^m(a) \pi^{m/2}} \right] \quad (7-b)$$

where, $\alpha = m/2 - 1$.

This relationship is based on an approximate assumption as the correction function $f(a)$ does not vary under constant amplitude stress.

The relationship among the material constants represented in the form of eq. (7) is obtained for homogeneous beams where the crack growth rate is isotropic. All the previous works conducted on fatigue crack growth rates dealt with almost homogeneous materials. Accordingly, it was questionable whether such relation could be applied to hybrid members consisting of different steel grades, since Gurney (19) indicated the relation of m and $\text{Log } C$ to be linear functions of yield stress of the material. The fracture surfaces observed in the present test, however, suggest the possibility of the application of the above relation, because it is recognized that the fatigue fracture surfaces indicate concentric circles as is typically shown in Fig. 8 and the fatigue crack growth rate may be isotropic.

Fisher et al. (14) also made an assumption to evaluate the crack growth constants, C and m , that the porosity was assumed to be described by a disc-like penny-shaped crack with a constant correction factor, $f(a)$, over the interval of integration of $2/\pi$.

In the present work, the initial crack radius, a_i , for the evaluation of the crack-growth constants, C and m , was assumed 0.5 mm that is the measured tip radius of elongated worm-holes. The final crack radius, a_f , was assumed to be the flange thickness. The equation of the mean regression line from the method of least squares applied to the test data for specimens failing from embedded weld defects in the longitudinal fillet weld is

$$\text{Log } N_f = 11.388 - 3.895 \text{ Log } S_r \quad \dots\dots\dots (8)$$

Thus, the material constants corresponding to C' and n in eq. (6) are 2.443×10^{11} and 3.895. From the above mentioned assumptions and eq. (7), the crack-growth constants, C and m , are evaluated and the fatigue crack growth-rate are represented numerically as

$$da/dN = 5.0 \times 10^{-12} \times (\Delta K)^{3.9} \quad \dots\dots\dots (9)$$

Eq. (9) as described from the mean regression curve of fatigue test data is shown in Fig. 10 and compared with the data points for the measured crack-growth rates on inside surface of the flange for growth as a three-ended crack. The data points are compared well with the estimated curve up to the ΔK of about $100 \text{ kg/mm}^{-3/2}$ where crack penetrates the extreme fiber of flanges. The derived crack-growth relationship given by Fisher et al. (14) and a conservative upper bound for growth-rates on ferrite-pearlite steels proposed by Barsom (18) are also compared with the present test results. These works gave the m -value of 3 and the one obtained by the present test was about 4 that is the preliminary proposed value by Paris (21). Kitagawa et al. (20) found a convenient correlation between C and m for a number of data obtained by different investigators. The correlation curve is expressed in the form of

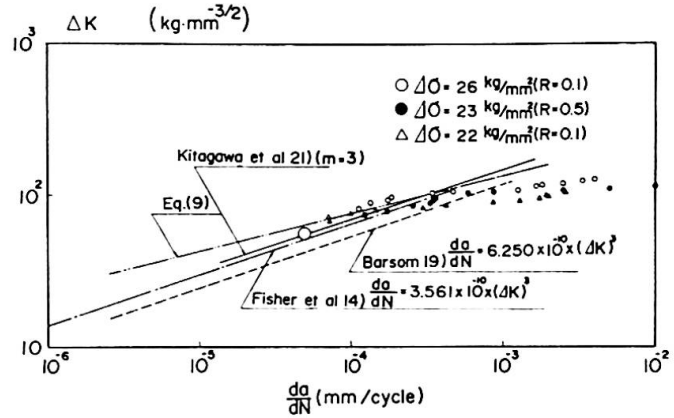


Fig. 10 Fatigue crack-growth rate

$$C = A/B^m \quad \dots\dots\dots (10)$$

where A and B are constants for some range of materials ; $A = 0.5 \times 10^{-4}$, $B = 55$ for steels and $A = 10^{-4}$, $B = 55$ for aluminium alloys. The crack-growth relationship derived from eq. (10) in case of $m=3$ is also shown in Fig. 10. It seems that the correlation given by eq. (10) is compared well with the one by Fisher et al. and predicts the conservative relation for the present test results. Despite the lack of data in the slower crack-growth rate region, these predictions give similar relations.

References

- 1) R. W. Frost and C. G. Schilling, ASCE, Proc., Vol. 90, No. ST3, June, 1964
- 2) H. S. Lew and A. A. Toprac, S. F. R. L. Tech. Rpt., p550-11, Janu., 1968
- 3) P. S. Carskaddan, Tech. Rpt. 57, 019-904(4), Applied Research Lab. U. S. Steel Corp.
- 4) R. W. Frost, Tech. Rpt., 57, 19-904(1), Applied Res. Lab., U. S. Steel Corp., Nov. 4, 1963
- 5) A. A. Toprac, Weld. J., May, 1969, 195-s 202-s
- 6) A. A. Toprac and M. Natarajan, ASCE, Proc., Vol. 97, No. ST4, 1971
- 7) Y. Maeda and Y. Kawai, 18th Conf. of Bridge and St. Eng. in Japan, p137
- 8) F. Nishino, M. Ito, M. Hoshino, JSSC, Vol. 7, No. 71, 1971 (in Japanese)
- 9) Y. Maeda, M. Ishiwata, Y. Kawai, IIW, Doc. XIII-734-74, April, 1974
- 10) Specs. for Highway Bridges, AASHTO, 1973
- 11) AISC Spec., Section 1.10, 1969, AISC
- 12) T. R. Gurney, Brit. Weld. J., July, 1962, p446
- 13) H. S. Reemsnyder, Weld. J., Oct., 1965, 458-s 465-s
- 14) M. A. Hirt, J. W. Fisher, Eng. Frac. Mech., 1973, Vol. 5, p415-429
- 15) J. W. Fisher, K. H. Frank, M. A. Hirt and B. M. Mcnamee, N. C. H. R. P., Rpt. No. 102, 1970
- 16) Y. Kikuchi and K. Yamada, JWS, Proc., Vol. 41, No. 9, 1972, p1085-1093
- 17) Interm Specs., Bridges, AASHTO., 1974
- 18) J. M. Barsom, U. S. Steel Corp., Applied Res. Lab., 1971
- 19) T. R. Gurney, Metal Const. and Brit. Weld. J., Feb., 1969, p91-96
- 20) H. Kitagawa et al., JSME, J, Vol. 75, 1972, p1068
- 21) P. C. Paris and F. Erdogan, ASME Trans., Vol. 85, Series D, No. 4, 1963

SUMMARY

The data of fatigue strength of Type 3 crack in hybrid girders which initiate at tension flanges were explored and fatigue crack propagation behaviour at tension flanges and webs was studied by fracture mechanics analysis.

RESUME

Les données de la résistance à la fatigue du Type 3 crack dans les poutres hybrides commençant par des brides de tension ont été explorées et le comportement propageur de craquelage par fatigue aux brides de tension et âmes a été étudié par l'analyse mécanique de fracture.

ZUSAMMENFASSUNG

Die Daten über Dauerfestigkeit des Anrisses vom Typ 3 an Hybridbalken, welche am Zuggurt beginnen, werden erörtert und das Ausbreitungsverhalten der Ermüdungsrisse an Zuggurten und Stegen werden mittels der Bruchmechanikanalyse untersucht.

Behaviour of Inelastic Beams under Cyclic Loading

Comportement de poutres sous l'effet de charges répétées

Verhalten von Trägern unter wiederholten Belastungen

SHOHKEN OGURA

Engineer

Izumi Sohken Engr.

Tokyo, Japan

YASUNAGA FUKUCHI

Associate Professor

Nagoya Institute of Technology

Nagoya, Japan

TADAO NAKAGOMI

Graduate Student

Tokyo Institute of Technology

Tokyo, Japan

HIROFUMI AOKI

Associate Professor

Yokohama National University

Yokohama, Japan

MORIHISA FUJIMOTO

Professor

Tokyo Institute of Technology

Tokyo, Japan

1. INTRODUCTION

In order to use higher strength steels advantageously in structures, many investigations have been carried out heretofore(1),(2). However, most of them have been on the strength and deformation capacity of the members under monotonous loading. In the countries which suffer from earthquakes frequently, such as Japan, the structural steel members are subjected to cyclically repeated loads. From this standpoint, the design methods which take into consideration the energy absorption due to plastic deformation should be adopted to design the structures economically and rationally. For this purpose, it is important to grasp thoroughly the inelastic behaviors of steel members subjected to extreme load reversals such as those which may occur during an earthquake. Investigations on the behavior of structures or structural members under cyclically repeated loads have been done considerably(3), especially in Japan(4). However, there has been little research done under such loads, relating to the phenomena of flange local buckling and lateral buckling, and little work, relating to the steels which have a yield point exceeding that of SM58 class steels.

This paper is a report of laboratory investigation of steel beams subjected to cyclically reversed loads under moment gradient, relating to flange local buckling and lateral buckling.

2. INELASTIC LOCAL BUCKLING BEAMS UNDER CYCLIC LOADING

2.1 SELECTIONS OF THE SPECIMENS

In Ref. 6, the limitation of width-thickness ratio b/t (where, b =one-half of flange width, t =thickness of flange) of wide-flange sections in the plastic designs is given as 6.00 for SM58(A572) class steels. In the case of beams under moment gradient, M.G. Lay has proposed next equation(8);

$$b/t = 1.78 / \sqrt{\sigma_y (3 + 1/Y) (1 + E/5.2E_{st}) E} \quad (2.1)$$

where, $Y = \sigma_y / \sigma_u$ = yield ratio of material (σ_u =tensile strength)

In Ref.7, the limitation of the ratio b/t in the elastic design is given as $b/t = 11.85$ for SM58(A572) class steels. The mechanical properties of materials are shown in Table 2.1, where ϵ_{st} =strain at initial strain hardening. Using the values of this table, $b/t = 4.20$ is obtained from Eq.(2.1).

From the basic data as described above, for the width-thickness ratio b/t of the test specimens, The values of 4.2, 6.0, 9.0, and 12.0 were used.

2.2 EXPERIMENTAL ARRANGEMENT AND METHOD

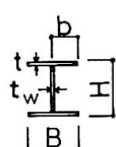
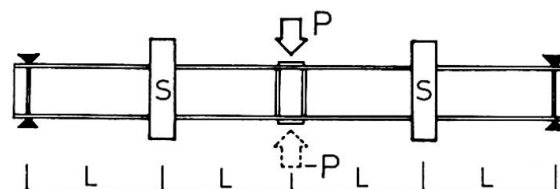
Local buckling tests were carried out on single-span simply supported beams with central concentrated loads applied on the top flanges, as shown in Fig. 1.1 (a). The test specimens are beams having the cross section shown in Fig. 1.1 (b). In Fig. 1.1 (a), the notation S shows the lateral support.

Unsupported length of a beam, L , is designed as the value of L/r_y is less than that recommended in Ref.6, i.e. $L/r_y = 43.9$ for the steels of $\sigma_y = 5.32t/cm^2$. The sectional dimensions of the test beams are given in Table 2.2, where, I =geometrical moment of inertia, and Z =section modulus. The program was made referring to experimental results in Ref.5.

According to Ref.5, in the beams having the same width-thickness ratio b/t , rotation capacity of the beam on which a monotonous loading test was performed showed the maximum value for all methods of loading, while the value of the beam subjected to cyclically repeated loads by controlling the deformations of the beam had the minimum value. In this report, therefore, three welded built up beams having the same ratio b/t were used (See Table 2.2). In Table 2.2, each beam is referred to by a code number such as SM9-3, in which SM stands for the materials of SM58, 9 means a width-thickness ratio of 9.0, and 3 means the third beam. The first beam test was carried out under monotonous loads, the second, under cyclically repeated loads by controlling the loads of the beam, i.e. the ratio of the positive moment to negative one was the ratio of 1:0.6 (See Fig. 2.2, 2.4 and 2.6), and the third, under cyclically repeated load by controlling the deformations of the beam (See Fig. 2.3, 2.5, 2.7 and 2.9).

Each so-called plastic cycle is defined here as the process of loading the beam downward until reaching $\delta/\delta_p = 2.5$ (where, δ = the deflections of the beam section at the midspan), unloading, then reverse loading the beam upward until reaching $\delta/\delta_p = -2.5$, in the case of the third beam. From the second excursion, in every process of loading the beam downward, the deflection of the beam at the midspan was increased with $\delta/\delta_p = 0.5$. The

deflections and the rotations of the beam at the midspan were measured with the dial gages and the strains were measured by means of wire strain gages for plastic region.



(a)

S shows the lateral support.

(b)

Fig. 1.1

Table 2.1
Mechanical Properties of Materials

σ_y $^{kcm^2}$	σ_u "	σ_y/σ_u	ϵ_y %	ϵ_{st} "	E $^{kcm^2}$	E_{st} "	E/E_{st}
5.32	6.19	.86	.252	2.06	2,111	25.2	83.7

Table 2.2
Sectional Dimensions

	H cm	B "	t "	t_w "	b/t	I cm ⁴	Z cm ³
SM12-2	21.76	21.56	.90	.61	11.98	4,629	425.4
3	21.80	21.59	.91	.61	11.86	4,695	430.7
3	21.73	21.56	.89	.62	12.11	4,580	421.5
SM9-2	21.80	16.17	.92	.61	8.79	3,649	334.8
3	21.83	16.18	.92	.62	8.79	3,669	336.0
3	22.30	16.17	.92	.62	8.79	3,845	344.8
SM6-2	21.86	10.79	.91	.60	5.93	2,559	234.1
3	21.77	10.77	.92	.62	5.85	2,564	235.6
3	21.83	10.78	.92	.60	5.86	2,569	235.4
SM4-3	9.74	7.58	.90	.59	4.21	292	60.0
3	9.76	7.57	.90	.58	4.21	293	60.0

Table 2.3 Experimental Results

	P_m "	P_{mp} "	P_m/P_{mp}	δ_m cm	δ_p "	δ_m/δ_p	θ_m/θ_p
SM12-2	53.7	50.03	1.07	2.54	.86	2.95	1.99
3	53.0	50.65	1.05	2.13	.86	2.48	1.86
3	53.4	49.63	1.08	2.15	.86	2.50	1.93
SM9-2	45.1	39.75	1.13	3.15	.87	3.62	2.54
3	43.7	40.20	1.09	3.01	.87	3.46	2.42
3	44.1	41.32	1.07	2.99	.86	3.48	2.22
SM6-2	32.5	28.17	1.12	4.49	.90	4.99	3.40
3	32.1	29.82	1.10	3.80	.90	4.22	3.31
3	33.0	29.22	1.14	3.30	.90	3.67	2.50
SM4-3	19.6	15.44	1.23	9.76	.62	15.74	5.93
3	17.8	15.44	1.15	3.75	.62	6.05	3.69

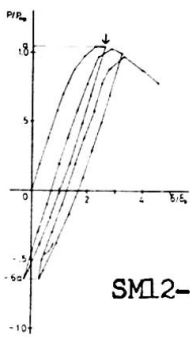


Fig. 2.2

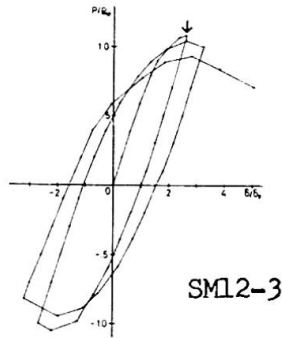


Fig. 2.3

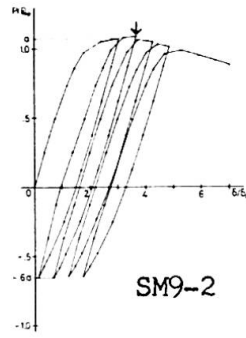


Fig. 2.4

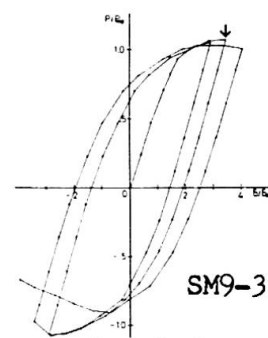


Fig. 2.5

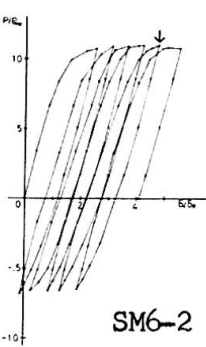


Fig. 2.6

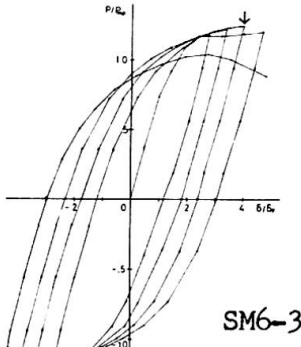


Fig. 2.7

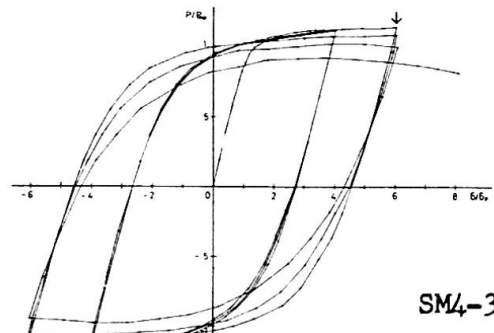


Fig. 2.8

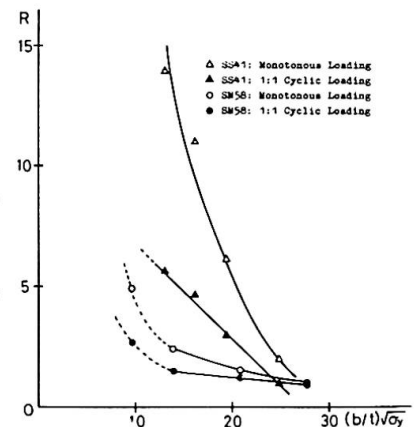
2.3 EXPERIMENTAL RESULTS

Experimental results are shown in Table 2.3, where P_m = maximum load, δ_m and θ_m = the deflection and rotation corresponding to P_m , respectively, P_{mp} = the load corresponding to full plastic moment, δ_p and θ_p = elastic deformation and rotation corresponding to P_{mp} , respectively. The P - δ curves are shown in Fig. 2.2 to Fig. 2.8. In each figure, the arrow shows the point of beam failure. From these figures, the rotation capacity of the beam in the plastic range was found to be very small. Especially, the negative slope of P - δ curves in the third beam became steep comparing with that of the first beam (monotonous loading test).

In Fig. 2.9, the relationships between R and $(b/t)\sqrt{\sigma_y}$ are shown together with the experimental

results of SS41 class steels. Fig. 2.9 shows that the rotation capacity of SM58 class steels is extremely small than that of SS41. In the case of the beams having the ratio b/t exceeding 6.0, as shown in Fig. 2.9, the rotation capacity of the beams decreases linearly as b/t becomes larger. However, in the case of the beam having the ratio $b/t=4.2$, the rotation capacity of the beams under monotonous loading was found to be 4.9, and 2.7 under cyclically repeated load. Therefore, the investigations relating to the beams having the ratio b/t between 4.2 and 6., need to be performed further. The rotation capacity of the beam under cyclically repeated loads was found to be very small, compared with that under monotonous loading. From the results, it is presumed that there are many problems in regard to the use of high strength steels to earthquake-proof structures.

It is very practically important to know the behavior of the members consisting of high strength steel and further research in this field is needed.



$R = \theta_m / \theta_p - 1$ = rotation capacity

Fig. 2.9 Relationships between R and $(b/t)\sqrt{\sigma_y}$

3. INELASTIC LATERAL BUCKLING UNDER CYCLIC LOADING

3.1 SPECIMENS AND EXPERIMENTAL METHOD

In this chapter, experiments of cyclic bending beams in which deformation capacity is determined by the combination of local and lateral buckling are presented. The experiments reported in this chapter were made by the Working Group of Fatigue in Low and High Cycle Range in Metals Subcommittee (The chairman is Prof. Morihisa Fujimoto) in Research Committee on Safety of Structural Materials (RCSSM, the chairman is Prof. Takeo Naka). Beam specimens were made of three kinds of structural carbon steel. Properties of the material are given in Table 3.1. Beam specimens were built up with steel plate of 9 mm by welding and the scope of the welding is illustrated in Fig. 3.1. After the specimens were welded, they were not treated by stress relief annealing. Dimensions of the specimens are given in Table 3.2. Ratio of width to thickness of flange, b/t , is restricted to one on each grade of steel, taking into consideration the experiments by G.H. Lay(9), T. Suzuki and so on, and recommendations of ASCE(6) and AIJ(7). Ratio of width to thickness of web, d/t_w is determined by the loading equipment, but it is within the values of the above recommendations.

The experimental purpose is to discuss the evaluation of deformation capacity of inelastic beams under cyclic loading, changing the variables such as slenderness factor $\lambda (=l_b/i_y)$, grade of steel and loading type. Conditions of loading and supporting are illustrated in Fig. 3.2. The specimen supported on rollers was loaded with a single concentrated load applied at the center, and deformable except for restricting to fall down sideways at loading and supported points. In fact, lateral buckling occurred symmetrically in all of specimens in two half-waves and the load reached maximum.

3.2 EXPERIMENTAL RESULTS

Fig. 3.3(SM50, $\lambda=55$) shows $M/M_p-\theta/\theta_p$ curves in cyclic loading as the amplitude was a rotational angle θ_m at maximum load M_m by monotonous loading, where M is applied moment, M_p , full plastic moment of the specimens, θ , rotation measured at supported point and θ_p , elastic rotation corresponding to M_p . And $M/M_p-\theta/\theta_p$ curve in cyclic loading between θ_m and $-0.6\theta_m$ is plotted in Fig. 3.4. And the curves in the case of SM50, $\lambda=45$ are plotted in Fig. 3.5 and 3.6. The $M/M_p-\theta/\theta_p$ curves (SM58, $\lambda=50$ and $\lambda=40$) in cyclic loading between $(1/2)\theta_m$ and $-(1/2)\theta_m$ are also plotted in Figs. 3.7 and 3.8. The endurance of beam in the case of SM58, $\lambda=50$ did not fall after 8 cycles loading, and that of SM58, $\lambda=40$ reached the maximum load in each cycle. $M/M_p-\theta/\theta_p$ curves (HW70, $\lambda=40$ and $\lambda=30$) under cyclic loading with amplitude between $(1/2)\theta_m$ and $-(1/2)\theta_m$ are plotted in Figs. 3.9 and 3.10.

After local buckling occurred at flange portion of every specimen, lateral buckling occurred. At the maximum load, local buckling the web portion was observed. It seems that the negative slope of $M/M_p-\theta/\theta_p$ curve after reaching the maximum load is determined by local buckling at web portion, especially under cyclic loading. The above experimental results indicated that the stability of hysteresis loop and deformational capacity of inelastic beams under cyclic loading are related to d/t_w as well as λ and b/t , when deformation capacity is prescribed by the combination.

Table 3.1

Chemical composition and Mechanical properties of Materials

Grade of steel	Chemical Composition (%)										Tension Test			Check Test					
	C	Si	Mn	P	S	Cu	Cr	Mo	V	B	Ceq	Y.P.	T.S.	El.	σ_y	σ_b	Est.	E_u	Est.
	x100				x1000					x100		kgf/mm ²	kgf/mm ²	(%)	kgf/mm ²	kgf/mm ²	(%)	kgf/mm ²	kgf/mm ²
SM 50	16	34	130	17	18							33	51	28	36.2	51.3	2.08	2.23	45.9
SM 58	14	24	140	22	6						38	62	69	25	60.9	66.7	1.75	7.44	27.6
HW 70	11	27	89	11	3	24	91	32	4	1	53	84	88	25	84.0	88.9		7.58	

Table 3.2 Dimension of Specimens and Experimental Results

Grade of steel	Specimen NO.	l (mm)	R (mm)	b (mm)	b/t	d (mm)	d/t	l_b (mm)	i_y (mm)	l_y/i_y	M_p (t·m)	θ_p (rad)	M_u/M_p	θ_u/θ_p	Loading condition
SM50	H5755M	8.86	9.8	63.0	7.10	282	31.9	1378	24.6	56.0	19.2	0.90	1.18	4.79	Monotony
	H5755C1	8.86	9.1	63.0	7.10	282	31.9	1378	24.7	55.9	19.0	0.90	1.16	4.47	$\theta_u \sim -\theta_u$
	H5755C2	8.86	10.5	63.2	7.13	282	31.9	1378	24.7	55.8	19.3	0.90	1.16	4.26	$\theta_u \sim -0.5\theta_u$
	H5745M	8.86	10.3	63.1	7.12	282	31.9	1130	24.7	45.8	19.3	0.74	1.22	7.77	Monotony
	H5745C1	8.86	10.2	62.9	7.10	283	31.9	1130	24.6	46.0	19.2	0.74	1.24	6.81	$\theta_u \sim -\theta_u$
SM58	H5745C2	8.86	10.4	63.2	7.13	282	31.8	1130	24.7	45.7	19.2	0.74	1.22	6.36	$\theta_u \sim -0.5\theta_u$
	H6650M	9.40	9.4	54.1	5.76	198	21.1	1130	22.3	50.7	19.5	1.79	1.05	3.51	Monotony
	H6650C1	9.40	9.2	54.4	5.79	198	21.1	1130	22.4	50.4	19.5	1.79			$0.7\theta_u \sim -0.7\theta_u$
	H6640M	9.40	10.2	53.9	5.73	198	21.1	904	22.1	40.9	19.6	1.43	1.10	5.53	Monotony
HW70	H6640C1	9.40	10.7	53.9	5.73	198	21.1	904	22.1	41.0	19.7	1.43			$0.6\theta_u \sim -0.6\theta_u$
	H7540M	9.48	11.7	45.4	4.79	126	13.3	805	19.6	41.0	14.4	2.63	1.06	4.88	Monotony
	H7540C1	9.48	10.4	45.3	4.78	126	13.3	805	19.7	41.0	14.0	2.60			$0.6\theta_u \sim -0.6\theta_u$
	H7530M	9.48	10.7	45.3	4.78	126	13.3	604	19.7	30.6	14.1	1.95	1.15	7.24	Monotony
	H7530C1	9.48	8.8	45.2	4.76	126	13.3	604	19.7	30.6	13.7	1.96			$0.6\theta_u \sim -0.6\theta_u$

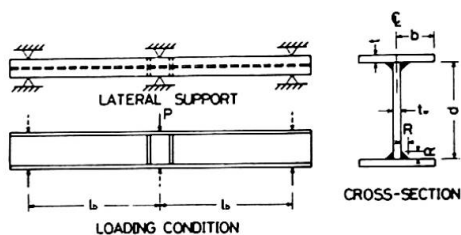


Fig. 3.1

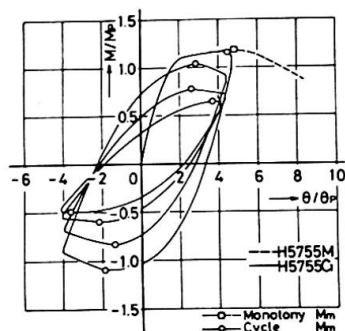


Fig. 3.3

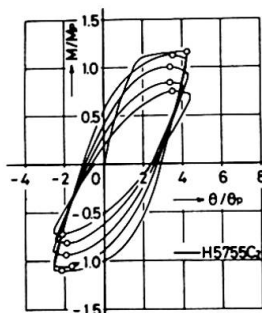


Fig. 3.4

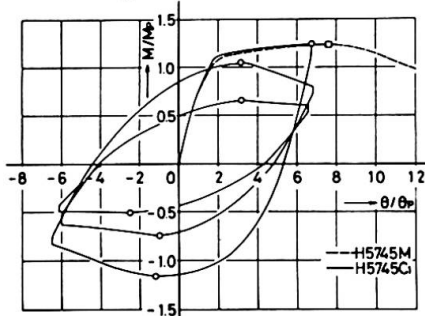


Fig. 3.5

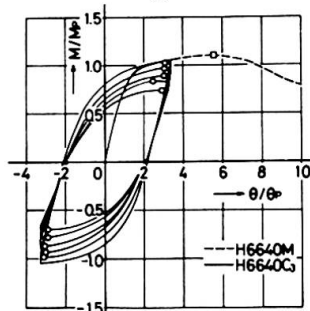


Fig. 3.8

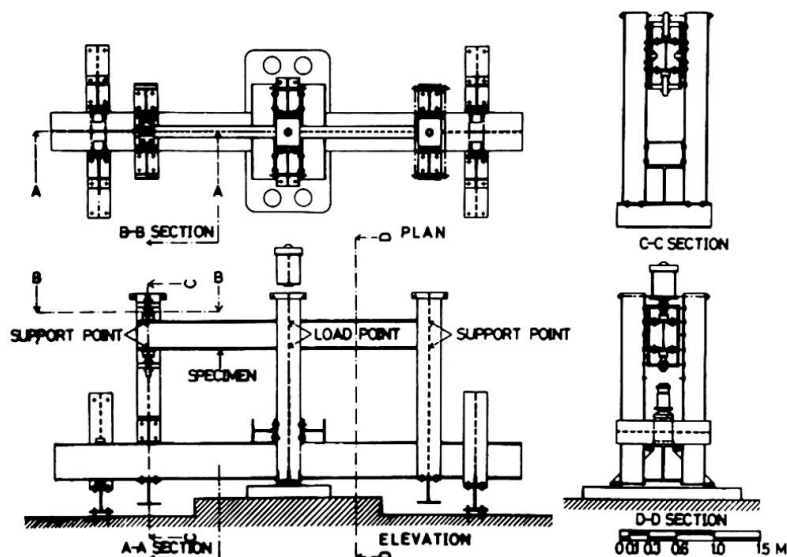


Fig. 3.2

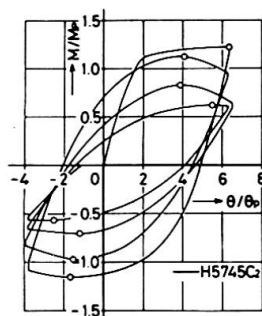


Fig. 3.6

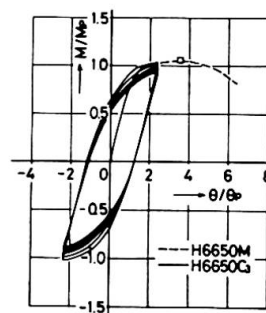


Fig. 3.7

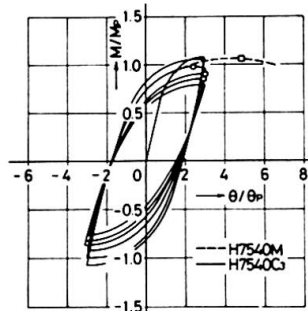


Fig. 3.9

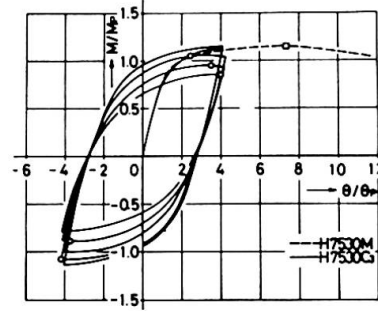


Fig. 3.10

ACKNOWLEDGEMENT

The authors wish to extend their appreciation to Prof. Ben Kato for his guidance.

REFERENCES

1. Adams, P.F., Lay, M.G. and Galambos, T.V. "Experiments on High-Strength Steel Members", WRC. Bulletin NO.10, Nov. 1965
2. Suzuki, T. and Ono, T. "Experimental Studies on the Plastic Design of High-Strength Steel Beams", Trans. AIJ. NO.219, May 1974, (in Japanese).
3. e.g. Bertero, V.V. and Popov, E.P. "Effect of Large Alternating Strains of Steel Beams", Proc. of ASCE, ST1, Feb. 1965
4. e.g. Suzuki, T., Tamamatsu, K., Kubodera, I. and Okuta, K. "Experimental Study on the Elasto-Plastic Behavior of Tensile Braced Frames", Tran. AIJ. NO.228 Feb. 1975, (in Japanese).
5. Fukuchi, Y. and Ogura, S. "Experimental Studies on Local Bucklings and Hysteretic Characteristics of H-Shape Beams", Trans. AIJ. NO.228, Feb. 1975, (in Japanese).
6. Plastic Design in Steel, A Guide and Commentary, 2nd Edition ASCE, 1971
7. AIJ. Specification for Design of Steel Structures, 1970
8. Lay, M.G. "Flange Local Buckling in Wide-Flange Shapes" J. of the Structural Division, Proc. of ASCE, ST6, Dec. 1965
9. Lay, M.G. and Galambos, T.V. "Inelastic Beams under Moment Gradient", J. of Structural Division Proc. of ASCE, ST1, Feb. 1967

SUMMARY

It was confirmed experimentally that rotation capacity of structural steel members, both mild and high strength steels, was influenced considerably by cyclic loading. The rotation capacity for beams of high strength steels with high yield ratio as compared with that of mild steels is small. The figures indicate that the rotation capacity of beams under cyclic loading is still lower. Therefore, it is desirable that the existing values L/r_y and b/t for high strength steels should be limited even more strictly.

RESUME

L'expérience confirme l'influence considérable de charges répétées sur la capacité de rotation d'éléments en acier doux et même à haute résistance. La capacité de rotation des poutres en acier à haute résistance et à haute limite d'élasticité est plus petite que celle de l'acier doux. Les figures montrent que la capacité de rotation des poutres sous charges répétées est encore plus petite. Par conséquent, il vaudrait mieux que les valeurs L/r_y et b/t en vigueur pour l'acier à haute résistance soient limitées sévèrement.

ZUSAMMENFASSUNG

Durch Versuche wurde festgestellt, dass die wiederholte Belastung auf die Rotationskapazität von Stäben sowohl aus leichtem wie aus hochfestem Stahl eine starke Wirkung ausübt. Die Rotationskapazität von Balken aus hochfestem Stahl mit hohem Streckungsverhältnis ist geringer als jene des weichen Stahls. Die Abbildungen zeigen, dass die Rotationskapazität der Balken unter wiederholter Belastung noch kleiner ist. Somit ist der bestehende Wert von L/r_y und b/t für hochfesten Stahl noch strenger zu begrenzen.

High Strength Steel Composite Beams with Formed Steel Deck

Poutres mixtes en acier à haute résistance avec platelage métallique

Hochfeste Verbundträger mit Stahlblechdecke

JOHN A. GRANT, Jr.
Research Assistant

JOHN W. FISHER
Professor of Civil Engineering
Fritz Engineering Laboratory, Lehigh University
Bethlehem, Pennsylvania, USA

ROGER G. SLUTTER
Professor of Civil Engineering

1. INTRODUCTION

During the past forty years, formed steel deck has become the most common floor system used in high rise steel frame structures. A natural consequence of this floor system was the development of composite action between the steel beam and the concrete slab by means of shear connectors welded through the deck to the beam flange. However when the corrugations of the deck run perpendicular to the beam, experimental results have shown that a reduction in beam capacity may ensue.

Initial studies of this condition were made on a proprietary basis for specific products in building applications and thus were uncoordinated. Consequently considerable variance among controlled parameters existed, making it difficult to draw any general conclusions. In 1967 a detailed study by Robinson(1) showed that for high, narrow ribs the shear capacity of the connector is a function of the rib geometry and is substantially less than the capacity of connectors embedded in a composite beam with a solid slab. In 1970, Fisher(2) summarized the investigations that had been conducted to date and proposed design criteria. Fisher concluded that composite beams could be modeled as having a haunched slab, equal in thickness to the solid part of the slab above the rib, except that the shear capacity of the connector is reduced. He modeled this reduction in shear capacity by the following formula:

$$Q_{rib} = A \cdot \frac{w}{h} \cdot Q_{sol} \leq Q_{sol} \quad (1)$$

where: Q_{rib} = shear strength of connection in a rib
 A_{rib} = numerical coefficient (0.5 for beam)
 w = average rib width
 h = height of rib
 Q_{sol} = shear strength of a connector in a solid slab

With the many uncontrolled and ill defined variables in these early investigations, there was a need for additional research in this area. Also there was virtually no experimental work done which considered the effect of high strength steel beams and the resulting effect of increased slab force on connector and beam capacity. A research program was initiated at Lehigh University in 1971 involving 17 full scale beam tests, 15 of which utilized high strength steel beams. The work reported herein includes a detailed analysis of these 17 composite beams. Additionally, this analysis is supplemented by an evaluation of 39 other beam tests reported by previous investigators. The work is described in detail in Ref. 3.

This report provides an evaluation of the shear capacity of stud connectors embedded in composite beams utilizing high strength steel with formed steel deck, as well as the flexural capacity of the composite beams themselves. Additionally the stiffness of composite beams with or without formed steel deck is evaluated for service loads.

2. DESCRIPTION OF TESTS

The experimental program at Lehigh consisted of tests on 17 simple span composite beams. The program was designed in accordance with the recommendations suggested in Refs. 2 and 4.

Series A consisted of six beams. It served as the basic series in the program, with average rib width - height ratios of 1.5 and 2. The beams were designed for partial shear connection. Series B consisted of two mild steel beams, as all other beams were high strength steel. Series C consisted of five beams with low degrees of shear connection (below 50%). Series D consisted of four beams with larger rib slopes as their major variable.

The test beams consisted of steel beams on simple spans of 24 or 32 ft. (7.31 to 9.75 m), acting compositely with concrete slabs cast on formed steel deck. All of the steel beams except two were W16 x 40 or W16 x 45 sections with yield strengths between 55 and 70 ksi (379.5 and 483.0 N/mm²). The two exceptions were both W16 x 58 sections with 36 ksi (248.4 N/mm²) yield.

The slabs of the beams were made with structural lightweight concrete conforming to the requirements of ASTM C330 (Specification for Lightweight Aggregates for Structural Concrete). The concrete strength and modulus of elasticity were maintained as constants within fabrication tolerances at 4.0 and 220 ksi (27.6 and 151800 N/mm²) respectively. Minimal reinforcement for all of the beams consisted of 6 x 6 - #10/10 welded wire fabric placed at mid-depth of the slab above the ribs. The thickness of the solid part of the slab was a constant 2-1/2 in. (63.5 mm) for all of the beams. The slab widths were proportioned as 16 times the full thickness of the slab plus the flange width of the steel beam. All slabs were cast without shoring.

The slabs were cast on 20 gauge galvanized steel deck without embossments. The rib heights of the deck were 1-1/2, 2 or 3 in. (38.1, 50.8 or 76.2 mm) for average rib width - height ratios of 1.5 and 2. The slopes of the ribs were a nominal 1 to 12 except for the series D beams which had 1 to 2 and 1 to 3 slopes. The steel deck was fabricated in widths of 24 or 36 in. (609.5 or 914.4 mm) with corresponding rib modules of 6 and 12 in. (152.4 and 304.8 mm).

Composite action between the steel beam and the slab was provided by the placement of 3/4 in. (19 mm) shear connectors. All studs conformed to ASTM A108 specification and were welded through the steel deck to the beam flange in a staggered pattern. All welds were tested by "sounding" the studs with a hammer. Questionable studs were given a 15 degree bend test. Faulty studs were replaced and retested. One or two studs were placed in a rib. The stud spacing was adjusted to accommodate the varying rib geometry but never exceeded 24 in. (609.5 mm). All studs were embedded 1-1/2 in. (38.1 mm) above the rib.

Four point loading was used on all of the beams to provide shear and moment conditions comparable to uniform load conditions. The loads were about equally spaced, but varied slightly so that loads were applied over a rib and not over a void. Figure 1 shows a typical test setup.

The beams were loaded in increments up to their estimated working load, then cycled ten times. After cycling the beams were reloaded in increments to near the ultimate load. Near ultimate, load was applied to produce fixed increments of deflection. Loading was terminated once the plateau of the load-deflection curve was established and deflections became excessive.

The beams were instrumented to measure the deflection at midspan, the slip

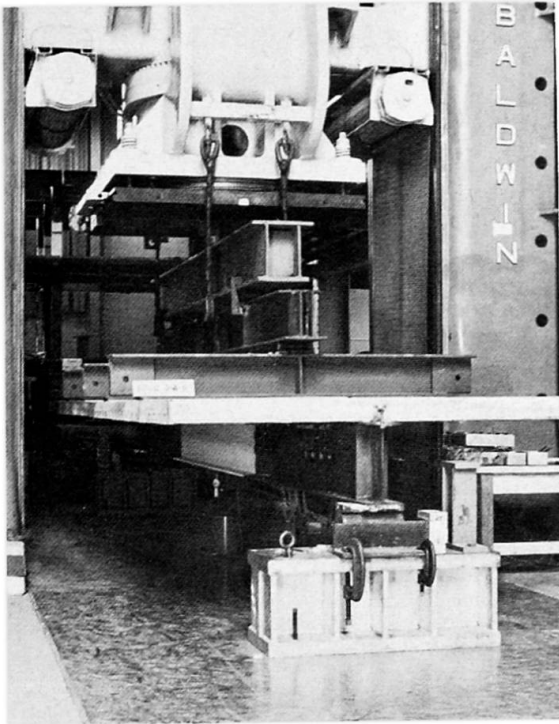


Fig. 1

at various points along the span, and the strain in the steel beam at various points along the span.

3. THEORETICAL CONSIDERATIONS

The flexural capacity of the test beams reported herein was determined essentially from the model suggested by Slutter and Driscoll(4) for composite beams with flat soffit slabs. However, the slab force was assumed to act at the centroid of the solid portion of the slab, above the top of the ribs and not at the center of the concrete stress block.

In many instances, the location of the slab force made little difference in the computed flexural capacity. For beams designed fully composite with the concrete slab governing the shear connection, the center of the stress block coincides with the centroid of the solid portion of the slab. However, for beams with low degrees of partial shear connection and/or high ribs, the location of the stress block has a significant influence on capacity.

For composite beams, with or without formed steel deck, there is loss of interaction or slip between the slab and the steel beam before developing the flexural capacity. This slip has little effect on the shear capacity of the connectors. However, it does effect the location of the slab force. Without any connection at all the compressive stress resultant would lie somewhere in the upper half of the full slab depth. However, with the bottom of the slab constrained by the presence of shear connectors the location of the stress resultant in the slab drops. The assumption that the stress resultant acts at the centroid of the solid portion of the slab seems to more adequately account for all cases involving composite beams with formed steel deck.

Robinson(5) has compared this difference in the assumed location of the slab force for a beam with 3 in. ribs and about 30% partial shear connection. He found that applying the method in Ref. 4 directly, provided an estimated capacity 3% higher than the test data and, that assuming the slab force to act at the center of the solid slab above the ribs, underestimated the capacity. However, he did not include the force on the shear connector directly under the load point, which falls at the edge of the shear span. Had this connector been included, the beam capacity would be overestimated by 9%. With the slab force acting at the center of the solid slab above the rib the capacity would be overestimated by 1%. Strain measurements on this beam confirm the location of the stress resultant in the slab as near the mid-depth of the solid portion of the slab. A similar conclusion was drawn from the Lehigh test beams.

4. BEHAVIOR OF COMPOSITE BEAMS WITH METAL DECK

4.1 Ductility - A significant aspect of these beams is their ductility. This ductility is demonstrated by the large deflections shown in the load-deflection plots in Fig. 2, even for beams with low degrees of partial shear connection. Also shown on the plots are two idealized elastic-plastic load-deflection curves. The elastic portion of the stiffer curve assumes complete interaction between the slab and the beam. The plastic plateau of that curve is the ultimate load for a partial shear connection with a reduced connector capacity defined in Eq. 1. The lower idealized curve is adjusted to account for an effective moment of inertia in the elastic range, which will be discussed later. The plastic plateau for that curve reflects a modified connector capacity as will be discussed later.

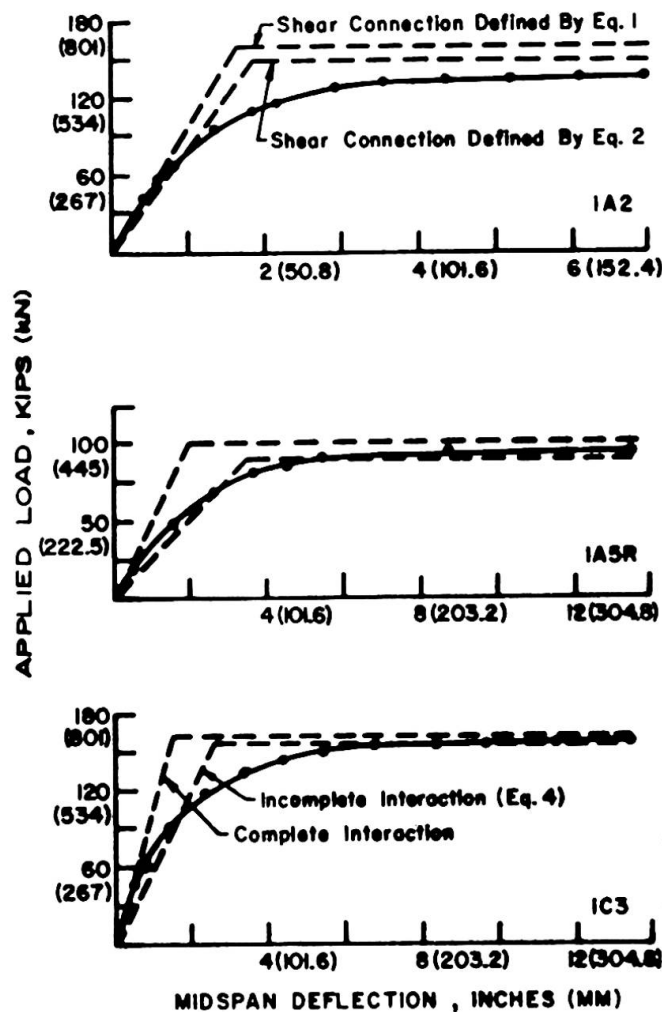


Fig. 2

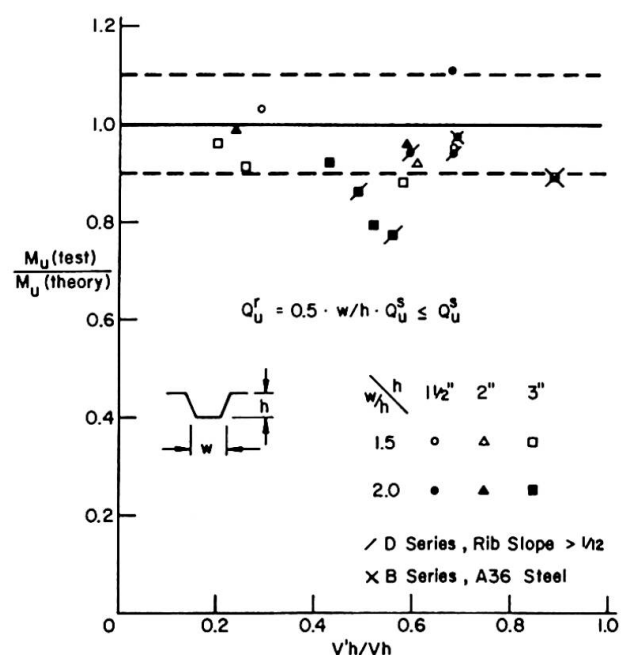


Fig. 3

All of the test beams sustained maximum deflections between 8 and 22 in. (203 to 560 mm). These deflections correspond to more than ten times the deflection at working load in all but two cases. Such large deflections were permitted by the formation of a plastic hinge near the mid-span in all of the beams. The formation of these plastic hinges which produced the desired ductility could only have been possible with a ductile shear connection.

Shear connectors were instrumented at selected points along each of the beams. Data on a few of the beams was analyzed and confirms the ductility of the shear connection. All exhibited ductile behavior which permitted the redistribution of the slab force along the span and thus a ductile composite beam. This redistribution of forces permits the prediction of an average connector capacity for the beam, such as suggested in Ref. 2.

The reason for the ductile behavior of the shear connector can be attributed to the relative wide slabs used in the Lehigh test beams. In these tests the slab widths were taken as 16 times the full thickness of the slab, including rib height, plus the width of the steel beam flange. Previous investigators(2,6) have suggested using this slab width for beam tests and for design because it provides an upper limit connector ductility and capacity and more closely simulates the slab-beam interaction in an actual structure. Strain measurements across the slab width have indicated that shear lag is no more severe in a ribbed slab than in a solid slab(3).

4.2 Flexural and Connector Capacity -

Unfortunately, the connector model suggested in Ref. 2 (see Eq. 1) for determining the flexural capacity of the composite beams proved unsatisfactory. Figure 3 shows the variation between test moment and theoretical moment using this model for all of the 17 beams. The test moment is nondimensionalized by the predicted moment and plotted against the degree of partial shear connection. Despite the obvious fact that several of the beams fall below their predicted capacity, the plot also shows that several beams with very low degrees of partial shear connection can obtain their predicted capacity. The observation has been made by Robinson(6) as well. Similarly rib slope and yield strength of the steel beam

did not appreciably effect the beam capacity, as can be seen in Fig. 3. It is apparent that the connector model must consider other variables.

One such variable was found to be the height of the rib. A reexamination of all available test data, indicated that all of the beams with 3 in. (76.2 mm) deck except one had a stud embedment length greater than 1-1/2 in. (38.1 mm) above the rib. Although not considered as a variable in the Lehigh test program, it was obvious that embedment length is a key parameter in connector capacity. This observation has also been made by Robinson(6).

Thus additional modifications to the connector capacity model proposed in Ref. 2 are required. Besides the average rib width - height ratio, the height of the rib and the embedment of the connector must be taken into account to correctly predict the flexural capacity of composite beams with formed steel deck. To reflect these additional governing parameters, the following revised model was developed:

$$Q_{rib} = 0.6 \cdot \frac{H-h}{h} \cdot \frac{w}{h} \cdot Q_{sol} \leq Q_{sol} \quad (2)$$

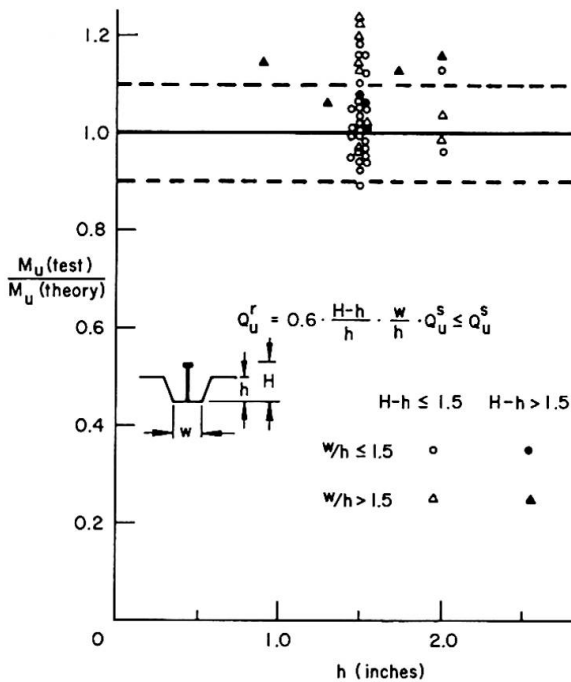
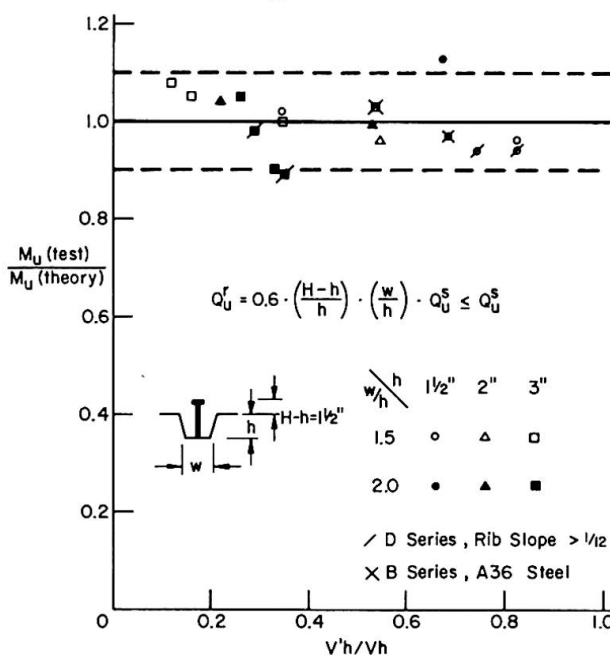


Figure 4 shows all 56 beam test results in terms of test moment nondimensionalized by theoretical moment as a function of rib height. Equation 2 was used in predicting beam capacity. Figure 5 shows the same moment ratio as a function of the degree of partial shear connection, $V'h/Vh$, but for the 17 Lehigh tests only. The plots indicate that the connector capacity defined by Eq. 2 provides a better estimate of flexural capacity for beams with 3 in. (76.2 mm) deck. About the same flexural capacity is provided for beams with 1-1/2 and 2 in. (38.1 and 50.8 mm) deck. Equation 2 continues to account for the varying width - height ratios as indicated by the relatively even dispersion of the test beams for all rib heights. Further details of this study are given in Ref. 3.



Early studies at the University of Illinois (8) and more recent studies at the University of Missouri (9) have shown that composite beams with flat soffit

slabs designed for full composite action have 85 to 90% of their calculated stiffness at the working load level. This loss in stiffness can be attributed to the fact that the shear connectors are flexible. Thus the connectors permit some slip or loss of interaction between the slab and the steel beam of a composite member, even though they will take all the force required for full composite action.

The shear connectors in a composite beam with formed metal deck behave similarly. Thus one would expect the same sort of difference to exist between actual and assumed stiffness of such beams designed for full composite action. The Lehigh test beams with the lowest degree of partial shear connection exhibited 20 to 30% loss of the stiffness which is about twice as much as experienced for full composite action in flat soffit slabs(8,9). On the other hand, these same beams provided at least twice the stiffness of a non-composite system. Thus a low degree of partial shear connection is very efficient in terms of stiffness.

Because of the complexity of the nonlinear variation of stiffness with the degree of partial shear connection, several empirical relationships have been examined(3). A relationship of the form:

$$I_{\text{eff}} = I_s + \frac{V'h}{V_h}^\alpha (I_{\text{tr}} - I_s) \quad (3)$$

where I_{eff} = effective moment of inertia
 I_s = moment of inertia of the steel section
 I_{tr} = moment of inertia of the transformed composite section
 α = numerical exponent

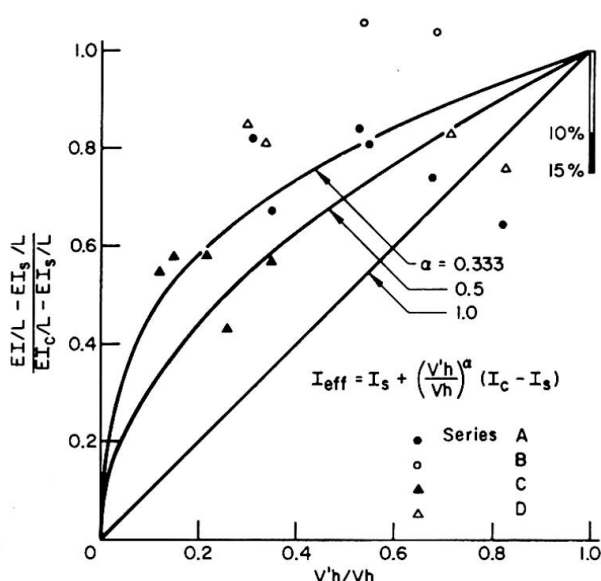


Fig. 6

was found to provide a reasonable fit to test data when α was taken equal to 1/2 or 1/3 as is demonstrated in Fig. 6. The stiffness provided by the 17 test beams is plotted for comparative purposes. With no shear connection, the stiffness is essentially that of the steel beam alone. A composite beam with full composite action (as provided by 100% shear connection) will be assumed to have the stiffness of a transformed section with no loss of interaction between slab and beam. The straight line running from 0 to 1 in Fig. 6 would represent a linear variation of stiffness with α equal to 1. The solid vertical line at $V'h/V_h$ equal to 1.0 shows the possible 15% variation between actual and assumed stiffness for a fully composite member. The plot clearly shows that the variation provided by the exponent α equal to 1/2 is generally conservative yet representative. The maxi-

mum deviation occurs as the degree of shear connection approaches unity. In no case is the loss of interaction greater than expected for a full shear connection.

Studies at the University of Missouri showed comparable behavior for composite beams with flat soffit slabs(9). A comparison of this data indicated general agreement with Eq. 3 when α was taken as 1/2.

5. CONCLUSIONS

The following conclusions may be drawn from the analysis reported herein:

1. The capacity of one or two stud shear connectors in the ribs of composite beams with formed steel deck may be determined from the following empirical expression:

$$Q_{\text{rib}} = 0.6 \cdot \frac{H - h}{l_r} \cdot \frac{w}{h} \cdot Q_{\text{sol}} \leq Q_{\text{sol}}$$

where H is the height of a stud shear connector in the rib, h is the height of the rib, w is the average rib width and Q_{sol} is the strength of the stud shear connector in a flat soffit slab.

2. The flexural capacity of a composite beam with formed steel deck can be more accurately and conservatively estimated if the slab force is considered to act at the mid-depth of the solid portion of the slab above the ribs, rather than at the centroid of the concrete stress block.

3. The flexural capacity of a composite beam utilizing high strength steel is not adversely affected by the increased slab force and can be predicted provided that the connector capacity is known.

4. The deflection of a composite beam with partial shear connection, with or without formed steel deck, may be estimated with the following expression for an effective moment of inertia:

$$I_{\text{eff}} = I_s + \frac{V'h}{V_h} (I_{\text{tr}} - I_s) \quad (4)$$

where I_s is the moment of inertia of the steel beam, I_{tr} is the moment of inertia of the transformed composite section, $V'h$ is the total horizontal shear to be resisted by connectors providing partial composite action and V_h is the total horizontal shear to be resisted by connectors under full composite action.

6. ACKNOWLEDGMENTS

The testing described in this report was conducted at Fritz Engineering Laboratory, Lehigh University. The contribution of the Fritz Laboratory staff is gratefully acknowledged.

7. REFERENCES

1. Robinson, H. - TESTS OF COMPOSITE BEAMS WITH CELLAR DECK, Journal of the Structural Division, ASCE, Vol. 93, No. ST4, August 1967.
2. Fisher, J. W. - DESIGN OF COMPOSITE BEAMS WITH FORMED METAL DECK, AISC Engineering Journal, AISC, Vol. 7, No. 3, July 1970.
3. Grant, J. A., Jr., Fisher, J. W. and Slutter, R. G. - COMPOSITE BEAMS WITH FORMED STEEL DECK, to be published, AISC Engineering Journal, AISC.
4. Slutter, R. G. and Driscoll, G. C. - FLEXURAL STRENGTH OF STEEL-CONCRETE COMPOSITE BEAMS, Journal of the Struc. Div., ASCE, Vol. 91, No. ST2, April 1965.
5. Robinson, H. - COMPOSITE BEAM INCORPORATING CELLULAR STEEL DECKING, Journal of the Structural Division, ASCE, Vol. 95, No. ST3, March 1969.
6. Robinson, H. and Wallace, I. W. - COMPOSITE BEAMS WITH PARTIAL CONNECTION, Meeting Preprint No. 1549, ASCE Annual Conf., St. Louis, Mo., Oct. 18, 1971.
7. Furlong, R. W. and Henderson, W. D. - REPORT OF LOAD TESTS ON COMPOSITE BEAMS OF LIGHTWEIGHT CONCRETE IN THREE-INCH METAL DECK WITH STUD LENGTH AS THE PRINCIPAL VARIABLE, University of Texas at Austin, August 1975.
8. Siess, C. P., Viest, I. M. and Newmark, N. M. - SMALL-SCALE TESTS OF SHEAR CONNECTORS AND COMPOSITE T-BEAMS, Bul. 396, Exp. Sta., U. of Ill., Urbana, Ill., 1952.
9. McGarraugh, J. B. and Baldwin, J. W. - LIGHTWEIGHT CONCRETE-ON-STEEL COMPOSITE BEAMS, AISC Engineering Journal, AISC, Vol. 8, No. 3, July 1971.

SUMMARY

This report presents the results of 17 composite beam tests conducted at Lehigh University incorporating formed steel deck. These results were analyzed in conjunction with 39 additional tests conducted by previous investigators. The purpose of this report was to evaluate shear connector capacity and beam flexural capacity and behaviour, particularly for beams utilizing high strength steel.

RESUME

Ce rapport contient les résultats de 17 essais réalisés à l'Université Lehigh sur des poutres mixtes avec platelage métallique incorporé. Ces résultats ont été analysés conjointement avec 39 autres essais réalisés auparavant par d'autres chercheurs. Le but de ce rapport était d'évaluer la résistance au cisaillement des boulons et la résistance à flexion des poutres, particulièrement pour les poutres en acier à haute résistance.

ZUSAMMENFASSUNG

Dieser Bericht enthält die Ergebnisse von 17 Tests an Verbundträgern, die an der Lehigh Universität durchgeführt wurden, an denen ein Stahlblech eingearbeitet war. Die Resultate wurden anhand 39 zusätzlicher Tests analysiert, die vorher von anderen Forschern ausgeführt wurden. Zweck dieses Berichtes war, die Tragfähigkeit der Verbundmittel und des Trägers selber, sowie das Verhalten, besonders für Tragbalken aus hochfesten Stählen, zu berechnen.